# Wave and vibration analysis of elastic metamaterial and phononic crystal beams with slowly varying properties

Adriano T. Fabro[a,*], Danilo Beli[b,c], Neil S. Ferguson[d], José Roberto F. Arruda[b], Brian R. Mace[e]

[a] *Department of Mechanical Engineering, University of Brasilia, Brasilia/Distrito Federal, Brazil*
[b] *School of Mechanical Engineering, University of Campinas, Campinas/São Paulo, Brazil*
[c] *São Carlos School of Engineering, University of São Paulo, São Carlos/São Paulo, Brazil*
[d] *Institute of Sound and Vibration Research, University of Southampton, Southampton, United Kingdom.*
[e] *Acoustics Research Centre, Department of Mechanical Engineering, University of Auckland, Auckland, New Zealand.*

**Abstract**

Periodic structures can be designed to exhibit wave propagation elastic band gap behaviour by varying material or geometrical properties, i.e. phononic crystals, or by periodically distributed resonators or boundary conditions, i.e. acoustic metamaterials, with various applications in passive noise and vibration control. However, variability in the manufacturing process causes material and geometry uncertainties that affect their band gap robustness and consequently their dynamic attenuation performance. In this work, the effects of slowly varying variability on the vibration suppression performance of metamaterials and phononic crystals is investigated. The spectral element and the wave and finite element approaches are used, assuming slowly varying properties, to model a beam with evenly spaced attached resonators and an undulating beam. In both cases, the band gap formation is investigated considering both non-uniform deterministic and spatially stochastic material and geometric variability. The proposed approach provides a framework to represent variability and randomness with spatial correlation of the periodic unit cell and then to assess their effects on the vibration suppression performance. It is shown that the spatial profile, or the correlation length in the case of random fields, plays a role on the band gap performance and that the presence of a critical section, i.e. a transition region between propagating and non-propagating waves, can significantly affect the band gap width and the amplitude of vibration attenuation.

*Keywords:* band gap, near-periodic structures, uncertainty analysis, WKB approximation, random field, slowly varying

## 1. Introduction

Phononic crystals and metamaterials are periodic structures that have been used to control and manipulate acoustic and elastic waves [1, 2, 3, 4]. Their applications include vibration attenuation [5, 6] and noise reduction [7, 8], acoustic cloaking [9], acoustic lenses [10] as well as mechanical topological waveguiding [11, 12]. One of their properties are the band gaps, which are frequency bands in which there exist a stop band effect [13]. While in phononic crystals the band gap is produced by Bragg scattering due to material or geometric periodic modulation [14], in metamaterials the band gap effect is created due to inclusions that work as internal resonators [15].

Typically, wave-based methods are used to calculate the complex dispersion diagram (free wave analysis) and the forced response in the frequency domain of a finite length periodic structure from the analysis of one single periodic cell. These formulations save computational time when compared to the standard full Finite Element (FE) method, thus providing a suitable framework for cases in which a large number of interactions is required, such as optimization and uncertainty analysis. Amongst the wave-based methods, the Spectral Element (SE) [16, 17] approach and Wave

*Correspondence should be addressed to A.T. Fabro

*Email addresses:* fabro@unb.br (Adriano T. Fabro ), dbeli@fem.unicamp.br (Danilo Beli), nsf@isvr.soton.ac.uk (Neil S. Ferguson), arruda@fem.unicamp.br (José Roberto F. Arruda), b.mace@auckland.ac.nz (Brian R. Mace)

and Finite Element (WFE) method [18, 19, 20] have been successfully used to model homogeneous and periodic structures in the past decades. The SE approach uses analytical solutions in a dynamic stiffness matrix framework, whilst the WFE method can benefit from any standard FE library to model a arbitrarily complex periodic cell [21, 22].

Manufacturing such structures from 3D printing has become one of the emerging topics in acoustic metamaterials because of their intrinsically complex geometry [23]. However, manufacturing processes introduce material and geometric uncertainties, possibly causing a disruption on the spatial periodicity required for the stop-band and pass-band features [24, 25] hence modifying the band gap performance [26, 27]. On the other hand, it has been known for decades that deterministic near-periodic structures can be designed in order to enhance their vibration/acoustic attenuation performance [28, 29, 30]. Near-periodic structures are referred herein as systems whose material or geometric properties vary spatially, following a deterministic function or a random field. This disruption of the spatial periodicity is known as disorder and results in the phenomenon known as localization [53]. It can be quantified by the average spatial decay of a travelling wave along the structure, the so-called localization factor [54]. Spatial variability in periodic structures, i.e., nearly periodic structures, can either prevent the band gap (stop band) formation [37, 55], or can be tuned to improve band gap effects when compared to those of the periodic structure [28, 56].

The effects of variability and randomness in phononic crystals and metamaterials have been investigated using different approaches. In some papers, it assumed that the periodic unit cell is uncertain, with no break of periodicity, and subsequently the stochastic response is calculated. Most of these analysis aims at providing a framework and design guidelines for metastructures. For instance, He et al. [31] proposed an stochastic analysis of acoustic metamaterials using a first order perturbation approach. Similarly, Wu et al. [32] also proposed a first order perturbation strategy along with interval parameter to evaluate the upper and lower bounds of acoustic metamaterials. Al Ba'ba'a et al. [33] investigated the effects of uncertainty on the unit cell parameters of elastic metamaterial using the polynomial chaos expansion. A Bayesian approach for wavenumber identification was proposed by Souza et al. [34] using experimental measurements in a elastic metamaterial produced from 3D printing. A derived analytical expression assuming an infinite number of identical resonators is used to estimate the material properties of the metastructure. It is shown that the band gap is the most uncertain region of the dispersion diagram, despite the metastructure being manufactured from the same material, and relate it to the break of periodicity not taken into account.

On the other hand, randomness and break of periodicity on the performance of metastructures have also been taken into account. Jia et al. [35] proposed a design approach for wide and robust band gaps in 2D phononic crystals. Randomness is included in the geometry of the unit cell and break of periodicity and symmetry is analysed in terms of combined deformation and manufacturing defects. Moreover, Achaoui et al. [36] show that Bragg scattering type of band gaps are less resilient to randomness than the locally resonant on two-dimensional pillars on a surface for hexagonal and honeycomb lattice symmetries. Sugino et al. [37] analysed the effects of randomness in both natural frequency and positioning of the resonators. They suggest that minimizing the variability is always beneficial for band gap widening. This is the opposite from what has been found by Celli et al. [38]. They show that random disorder can be used for band gap widening, which suggests that some underlying physics is not well explored.

For slowly varying structures, the WKB approximation can be used. This formulation was first proposed by Jeffreys [39] and latter by Wentzel, Kramers and Brillouin, who gave their name to the method, for solving the Schrodinger equation in quantum mechanics [40]. The WKB approximation assumes slowly varying properties such that internal reflections due to local impedance changes are negligible [41, 42]. It has the advantage of maintaining a wave-like approach and can be used for calculating the forced response of non-homogeneous structures using a very similar approach to that for homogeneous structures [43]. The WKB approach was employed to study tunnelling in quantum systems [44] and acoustic waves [45] as well as to compute incident, reflected and transmitted gravitational waves for black-holes [46]. More recently, in structural mechanics, the WKB method has been used to investigate curved rods with slow diameter variation [47], beams with spatially correlated random properties [43], and elastic waves in a shell of revolution [48]. Typically, the WKB approximation is restricted to analytical solutions, but its physical interpretation in terms of energy conserving properties [42, 47] can be used along with wave-based numerical approaches, such as WFE and SE [49, 50, 51]. Spatially correlated randomness can be represented by a second order homogeneous random field using the Karhunen-Loeve (KL) expansion [52], in which the spatial smoothness is given by a correlation length, thus it can be slowly varying.

Even though the effects of correlated disorder in periodic systems have been previously investigated (e.g. [57, 27, 29]), and the WKB approximation have been used to investigate nearly-periodic structures [58, 59], very little work has been done on investigating its effects on the wave coupling (locking phenomenon) and locally resonant type band

gap formation in other branches of physics (e.g. [60, 61]) and on structural dynamics applications. For instance, Zhu et al. [62] have proposed the first experimental demonstration of acoustic rainbow trapping, i.e., a metamaterial that traps broadband acoustic waves. Chen et al. [63] have applied this concept to a gradient metamaterial in order to observe the enhancement of flexural waves in beams and Meng et al. [64] have propose a optimization approach for improved vibration attenuation considering the resonators profile in a broadband multifrequency metastructure, with experimental demonstration.

The aim of this work is to investigate the effects of slowly varying properties and spatially correlated randomness on the vibration suppression performance from metamaterials and phononic crystals. Both SE and WFE approaches are used under the assumptions of the WKB approximation for slowly varying properties [42, 51]. The former is used to model a beam with evenly attached resonators and the latter is used in an undulated beam. The band gap formation of both straight beams with attached resonators [65, 66] and undulated beams [67] are investigated considering non-uniform deterministic and spatially stochastic material and geometric variability. The band gap in the undulated beam is due to the wave coupling (locking phenomenon), i.e. a phononic crystal, and in the straight beam is due to the resonators, i.e. a metamaterial. The novelty of the proposed approach relies on providing a framework to represent variability and randomness with spatial correlation of the periodic unit cell and then to quantify their effects on the vibration suppression performance.

In the next section, the theoretical background for the dynamic analysis of near-periodic structures using the SE and WFE methods under the slowly varying assumption is presented. Section 3 presents the formulation of the periodic and near-periodic metamaterial beam and the effects of near-periodicity and randomness of its vibration attenuation performance. Spatially correlated randomness is introduced by the KL expansion and the effects of different correlation lengths, a measure of the scale of the spatial fluctuation, are explored. A similar analysis is further extended for an undulating beam in Section 4 with varying material and geometrical properties. Finally, concluding remarks are given in Section 5.

## 2. Deterministic analysis by a wave-based approach

This section reviews a formulation for the analysis of wave propagation in periodic structures in terms of the dynamic stiffness of a single unit cell. Moreover, it presents a formulation introduced by Fabro et al. [49, 51] for the forced response of non-homogeneous waveguides with slowly varying properties, which is then applied to nearly-periodic structures.The proposed slowly varying approach is on based the conservation time-averaged energy flow, which is in principle equivalent to the WKB approximation to its leading order, as described by Pierce [42], for inhomogeneous beams and plates. Recently, Nielsen and Sorokin [47] have also shown that the energy flux conservation property leads to the exact amplitude function to the leading order of the approximation with applications to Rayleigh and Timoshenko beam theories in curved waveguides and Morsbøl et al. [68] have presented similar results for elastic waves on a shell of revolution. Most importantly, this indicated that the WKB approximation can be used to find a suitable generalization of the wave solution in terms of the change of phase and amplitude without the need of an explicit analytical solution.

### *2.1. Complex free wave propagation along a period structure: the eigenvalue problem*

The first step is modeling the unit cell with SE [16, 69] or FE [70]. In Fig. 1 a unit cell with one-dimensional periodicity is considered where left (L), right (R) and interior (I) degrees of freedom (DOFs) are presented. The equation of motion for the $s^{th}$ unit cell described in the frequency domain is $\widetilde{\mathbf{D}}\hat{\mathbf{q}} = \hat{\mathbf{f}}$, where $\hat{\mathbf{q}}$ is the discrete displacement/rotation vector composed by all degrees of freedom, $\hat{\mathbf{f}}$ is the vector of corresponding internal forces and $\hat{(\ )}$ represents the time harmonic description. If no external forces are applied to the interior DOFs, $\hat{\mathbf{f}}_{\mathtt{I}} = \mathbf{0}$, these DOFs can be related to the left and right interface DOFs by $\hat{\mathbf{q}}_{\mathtt{I}} = -\widetilde{\mathbf{D}}_{\mathtt{II}}^{-1}(\widetilde{\mathbf{D}}_{\mathtt{IL}}\hat{\mathbf{q}}_{\mathtt{L}} + \widetilde{\mathbf{D}}_{\mathtt{IR}}\hat{\mathbf{q}}_{\mathtt{R}})$ [71] and a condensed dynamic stiffness matrix is obtained such that

$$\begin{bmatrix} \mathbf{D}_{\mathtt{LL}} & \mathbf{D}_{\mathtt{LR}} \\ \mathbf{D}_{\mathtt{RL}} & \mathbf{D}_{\mathtt{RR}} \end{bmatrix} \begin{bmatrix} \hat{\mathbf{q}}_{\mathtt{L}} \\ \hat{\mathbf{q}}_{\mathtt{R}} \end{bmatrix} = \begin{bmatrix} \hat{\mathbf{f}}_{\mathtt{L}} \\ \hat{\mathbf{f}}_{\mathtt{R}} \end{bmatrix}, \tag{1}$$

where $\mathbf{D}_{\mathtt{BB}} = \widetilde{\mathbf{D}}_{\mathtt{BB}} - \widetilde{\mathbf{D}}_{\mathtt{BI}}\widetilde{\mathbf{D}}_{\mathtt{II}}^{-1}\widetilde{\mathbf{D}}_{\mathtt{IB}}$, with $\mathtt{B} = [\mathtt{L} \quad \mathtt{R}]$.

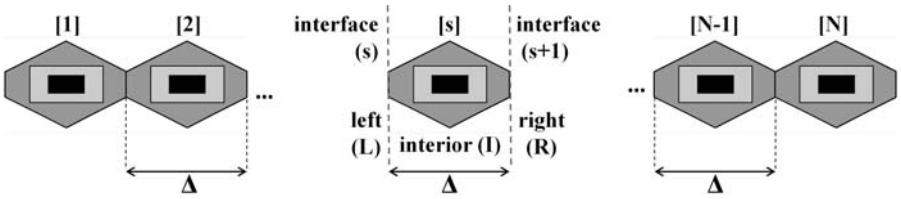


Figure 1: One-dimensional periodic structure with a symmetric unit cell.

By assuming the periodic structure to be free of external forces, the compatibility of displacements as well as the equilibrium of internal forces at the interface of two consecutive unit cells are given by $\hat{\mathbf{q}}_{\mathtt{R}}^{(s)} = \hat{\mathbf{q}}_{\mathtt{L}}^{(s+1)}$ and $\hat{\mathbf{f}}_{\mathtt{R}}^{(s)} = -\hat{\mathbf{f}}_{\mathtt{L}}^{(s+1)}$, respectively. In addition, the state vector of two consecutive interfaces can be related by a transfer matrix which is written in terms of the condensed dynamic stiffness matrix as

$$\mathbf{u}^{(s+1)} = \mathbf{T}\mathbf{u}^{(s)}, \tag{2}$$

where

$$\mathbf{T} = \begin{bmatrix} -\mathbf{D}_{\mathtt{LR}}^{-1}\mathbf{D}_{\mathtt{LL}} & \mathbf{D}_{\mathtt{LR}}^{-1} \\ -\mathbf{D}_{\mathtt{RL}} + \mathbf{D}_{\mathtt{RR}}\mathbf{D}_{\mathtt{LR}}^{-1}\mathbf{D}_{\mathtt{LL}} & -\mathbf{D}_{\mathtt{RR}}\mathbf{D}_{\mathtt{LR}}^{-1} \end{bmatrix}, \quad \mathbf{u}^{(s+1)} = \begin{bmatrix} \hat{\mathbf{q}}_{\mathtt{L}}^{(s+1)} \\ \hat{\mathbf{f}}_{\mathtt{L}}^{(s+1)} \end{bmatrix} \quad \text{and} \quad \mathbf{u}^{(s)} = \begin{bmatrix} \hat{\mathbf{q}}_{\mathtt{L}}^{(s)} \\ \hat{\mathbf{f}}_{\mathtt{L}}^{(s)} \end{bmatrix}.$$

If the dynamic stiffness matrix is symmetric then $\mathbf{T}$ is symplectic; moreover, $\mathbf{T}$ is $\Delta-$periodic ($\Delta$ is the length of the unit cell), which makes this matrix invariant under a translation of length $\Delta$ [72]. Due to the periodicity, Bloch's theorem can be applied to relate the state vectors at two consecutive interfaces, $\mathbf{u}^{(s+1)} = \lambda\mathbf{u}^{(s)}$, where $\lambda_j = e^{-\mathrm{i}\mu_j}$ and where $\mu_j$ is the propagation constant. Therefore, the eigenvalue problem in Eq. (2) becomes

$$\mathbf{T}\boldsymbol{\phi}_j = \lambda_j\boldsymbol{\phi}_j. \tag{3}$$

The previous eigenproblem provides $2n$ eigensolutions, where $n$ corresponds to the number of DOFs associated with each interface. While the eigenvalues ($\lambda_j$) are associated with the phase change and/or attenuation along the structure, the eigenvectors or wave mode shapes ($\boldsymbol{\phi}_j$) indicate the spatial distribution of the DOFs and forces at the interface [18]. The wave modes appear in pairs ($\lambda_j^+$, $\boldsymbol{\phi}_j^+$) and ($\lambda_j^-$, $\phi_j^-$), which are related to the right-going and left-going waves, respectively. Also, because $\widetilde{\mathbf{D}}$ is symmetric, the eigenvalues related to forward and backward going waves are related by $\lambda_j^- = 1/\lambda_j^+$. Moreover, the eigenvectors can be partitioned in DOF and force components as $\boldsymbol{\phi}_j^{\mathtt{T}} = [\boldsymbol{\phi}_{qj}^{\mathtt{T}} \quad \boldsymbol{\phi}_{fj}^{\mathtt{T}}]$ and the right-going waves are defined such that $|\lambda_j^+| \leq 1$ and $\Re\{i\omega\boldsymbol{\phi}_{fj}^{\mathtt{T}}\boldsymbol{\phi}_{qj}\} < 0$ if $|\lambda_j^+| = 1$. The eigenvalue problem computed by the transfer matrix can be ill-conditioned leading to numerical issues for the computation of the eigenvalue problem which can be circumvented by restating the eigenproblem in a better conditioned way and enforcing analytical relations between positive and negative going travelling waves [73, 74, 21] of the symmetric unit cell or by using the symplectic properties for the case of non-symmetric unit cells [22].

Tracking the wave modes in frequency is crucial to understand the wave propagation behaviour given that the analysis provides eigensolutions at discrete frequencies. Moreover, this step is fundamental to compute the phase change in the slowly varying WKB approach, which will be shown in the next subsection. By considering two sequential frequencies close to each other, the wavemode at $\omega_{i+1}$ that represent the same branch of the dispersion curves at $\omega_i$ is such that

$$\left| \frac{\phi_j(\omega_i)^H}{\|\phi_j(\omega_i)\|} \frac{\phi_j(\omega_{i+1})}{\|\phi_j(\omega_{i+1})\|} \right| = \max_p \left\{ \left| \frac{\phi_j(\omega_i)^H}{\|\phi_j(\omega_i)\|} \frac{\phi_p(\omega_{i+1})}{\|\phi_p(\omega_{i+1})\|} \right| \right\}, \tag{4}$$

where $(.)^H$ is the conjugate transpose. This has been termed as the Wave Assurance Criterion (WAC) [75]. The two frequencies need to be close enough to properly resolve the branches of the dispersion curves. This is particularly problematical close to critical frequencies where two branches are close together due to wave veering or locking [76] or where wave modes cut-on. Alternatively, the symplectic orthogonality properties of the wave can also be used as a

tracking criterion [74].

*2.2. Forced response of nearly-periodic structures with slowly varying properties*

In this section, the procedure to compute the response due to a point time harmonic forcing of nearly-periodic structures with slowly varying properties is briefly presented. Assuming time harmonic motion, a linear transformation can be used to relate the physical domain to the wave amplitude domain [20]

$$\hat{\mathbf{q}}_{\mathtt{L}} = \mathbf{\Phi}^{+}_{\mathtt{q}}\mathbf{a}^{+} + \mathbf{\Phi}^{-}_{\mathtt{q}}\mathbf{a}^{-} \quad \text{and} \quad \hat{\mathbf{f}}_{\mathtt{L}} = \mathbf{\Phi}^{+}_{\mathtt{f}}\mathbf{a}^{+} + \mathbf{\Phi}^{-}_{\mathtt{f}}\mathbf{a}^{-}, \tag{5}$$

in terms of the positive going $\mathbf{a}^{+}$ and negative going $\mathbf{a}^{-}$ wave amplitudes, and the matrices $\mathbf{\Phi}^{\pm}_{\mathtt{q}} = [\boldsymbol{\phi}^{\pm}_{q1} \cdots \boldsymbol{\phi}^{\pm}_{qm}]$ and $\mathbf{\Phi}^{\pm}_{\mathtt{f}} = [\boldsymbol{\phi}^{\pm}_{f1} \cdots \boldsymbol{\phi}^{\pm}_{fm}]$ are $n \times m$, where $n$ is the number of DOF in the left interface and $m$ corresponds to the number of retained wavemodes. For a periodic structure, the wave modes are the same for any periodic cell while in the nearly periodic case they depend on the position.

It is assumed that the positive and negative propagation matrices for waves propagating from 0 to $L = N\Delta$, i.e. across N unit cells, can be written as [77]

$$\mathbf{\Lambda}^{+}(0, L) = \mathtt{diag}\left[\exp\left(-\mathrm{i}\theta_j(0, L) + \gamma_j(0, L)\right)\right] \tag{6}$$

$$\mathbf{\Lambda}^{-}(L, 0) = \mathtt{diag}\left[\exp\left(-\mathrm{i}\theta_j(0, L) - \gamma_j(0, L)\right)\right], \tag{7}$$

where $\mathtt{diag}[\cdot]$ stands for a diagonal matrix, $\theta_j(0, L)$ is the total phase change and wave attenuation of the $j^{th}$ wave mode, given by

$$\theta_j(0, L) = \sum_{i=1}^{N} \Re\left[\mu_j(x_i)\right] + \mathrm{i}\sum_{i=1}^{N} \Im\left[\mu_j(x_i)\right], \tag{8}$$

with $\mu_j(x_i)$ being the locally defined propagation constant at the position $x_i$ of the centre of the $i^{th}$ unit cell. Moreover, $\Re\left[\mu_j(x_i)\right]$ is related to the phase change, $\Im\left[\mu_j(x_i)\right]$ is related to wave attenuation and damping and $\gamma_j(0, L)$ is the amplitude change caused by the non-periodic changes on the structure.

This assumption considers that negligible wave reflection occurs due to the slowly varying near-periodicity. Moreover, it is also assumed that there are no critical sections, also known as turning points in the WKB approach, which can arise from the rapidly changing properties, due to waves cutting-on/off and due to waves veering or locking [76]. It can also be shown that this is equivalent to assuming that systems undergoes no significant localization over lengths scales of order $L = N\Delta$ [59]. Note that $\mathbf{\Lambda}^{+}(0, L) \neq \mathbf{\Lambda}^{-}(L, 0)$, unlike the periodic case. The real part of $\theta_j(0, L)$ is related to the phase change and the imaginary part of $\theta_j(0, L)$ is related to the wave attenuation due to damping. Both SE and WFE methods can be used to estimate a local propagation and respective wave modes. This is analogous to the assumption made in the WKB method for propagation along a continuous waveguide, but here rephrase for a near periodic structure.

Due to the slowly varying assumption, the locally defined propagation constant can be approximated to a continuously varying function

$$\mu_j(x_i) \approx \mu_j(x). \tag{9}$$

Typically, this approximation is valid if the essential features of the spatial variability, which can be expressed in terms of the spatial frequency are suitably captured. The slowly varying assumption is equivalent to assuming that the wavelengths are small when compared to the spatial frequency content [77]. When considering spatially correlated random variability (see Appendix A), the spatial correlation length should be taken into account. It can be shown that the spatial frequency of the random field increases with the increasing order the KL expansion and that each term of the series have a equivalent spatial frequency representation [78, 79]. The proposed approximation is equivalent to a mid-point type of random field discretization. Therefore, it is recommended as a rule of thumb that the unit cell size $\Delta$ is at least four times smaller than the random field correlation length $b$.

This approximation can be done from a polynomial interpolation.Therefore, a numerical scheme such as Gauss-Legendre (GL) quadrature can be used to approximate the phase change as

$$\theta_j(0,L) \approx \sum_{m=1}^{N_{gl}} G_i \Re\left[\mu_j(x_m)\right] + \mathrm{i} \sum_{m=1}^{N_{gl}} G_i \Im\left[\mu_j(x_m)\right], \tag{10}$$

where $G_i$ are the weights and $\mu_j(x_m)$ is the $j^{th}$ propagation constant given at the sampling point $x_m$, defined from the GL quadrature, and $N_{gl}$ is the number of integration points. This strategy is proposed to keep the number of evaluations of the propagation constant to a minimum and then avoid excessive computational cost.

The amplitude change due to non-periodic changes on the structure can be calculated from energy conservation for an undamped system as a consequence of the WKB approximation [42]. It can be shown that the two approaches are equivalent to the leading order of the WKB approximation [45, 48]. Therefore, for a positive-going wave travelling from $x_a$, with amplitude $\mathbf{a}^+$, to $x_b$, with amplitude $\mathbf{b}^+$, assuming no damping, the time average power transmitted through the cross-sections, at the two positions must be equal, leading to [51]

$$\gamma_j(0,L) = \frac{1}{2}\log\left\{\frac{\Re\left[\mathrm{i}\omega\boldsymbol{\phi}_{f,i}^{+H}(0)\boldsymbol{\phi}_{q,i}^{+}(0)\right]}{\Re\left[\mathrm{i}\omega\boldsymbol{\phi}_{f,i}^{+H}(L)\boldsymbol{\phi}_{q,i}^{+}(L)\right]}\right\}. \tag{11}$$

Note that, although the wave modes propagate independently, the wave mode shapes $\boldsymbol{\phi}_i^{\pm}(x)$ vary slowly along the structure. It is also assumed that light damping can be included straightforwardly by calculating the complex wavenumber $k_j(x)$ at each segment using the WFE or SE approaches and then Eq. (10) is applied to calculate the total phase change and attenuation. In the following sections, this approach is applied to both a metastructure and to a phononic crystal, both with nearly-periodic properties. The effects of the break of periodicity are investigated assuming slowly varying properties.

The response to a point force can be considered as illustrated in Fig. 2, thus

$$\mathbf{c}^+ = \mathbf{e}^+ + \mathbf{a}^+, \tag{12}$$

where $\mathbf{c}^+$ is the outgoing wave and $\mathbf{e}^+$ is the amplitude of the wave directly generated by the forcing applied at the left boundary and $\mathbf{a}^+$ is the wave amplitude produced by reflection of $\mathbf{a}^-$ incident at the boundary. The latter can be calculated directly from equilibrium and continuity conditions and Eq. (5). Moreover, wave amplitudes at the left and right ends are related by the reflection matrices as $\mathbf{a}^+ = \mathbf{r}_{\mathrm{L}}\mathbf{a}^-$ and $\mathbf{b}^- = \mathbf{r}_{\mathrm{R}}\mathbf{b}^+$. The travelling wave amplitudes are related by the propagation matrices as $\mathbf{b}^+ = \boldsymbol{\Lambda}^+(0,L)\mathbf{a}^+$, $\mathbf{a}^- = \boldsymbol{\Lambda}^-(L,0)\mathbf{b}^-$. The forced response at the right boundary can be calculated using Eq. (5) and the wave amplitudes given by

$$\mathbf{b}^+ = \left(\mathbf{I} - \boldsymbol{\Lambda}^+(0,L)\mathbf{r}_{\mathrm{L}}\boldsymbol{\Lambda}^-(L,0)\mathbf{r}_{\mathrm{R}}\right)^{-1}\left(\boldsymbol{\Lambda}^+(0,L)\mathbf{e}^+\right) \tag{13}$$

$$\mathbf{b}^- = \mathbf{r}_{\mathrm{R}}\mathbf{b}^+. \tag{14}$$

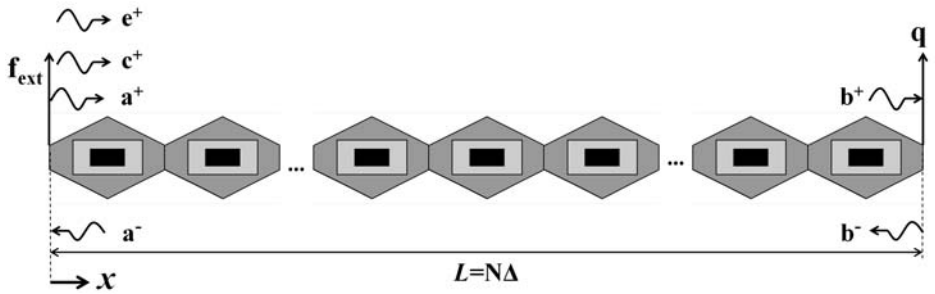


Figure 2: Point excitation and wave amplitudes on a periodic structure with slowly varying properties.

In general, the boundary conditions can be represented by $\mathbf{Af} + \mathbf{Bq} = \mathbf{0}$. Thus, the reflection matrices at the left and right ends are calculated from [80, 20] as

$$\mathbf{r}_{\mathtt{L}} = -\left(\mathbf{A}\boldsymbol{\Phi}_{\mathtt{f}}^{+} + \mathbf{B}\boldsymbol{\Phi}_{\mathtt{q}}^{+}\right)^{-1}\left(\mathbf{A}\boldsymbol{\Phi}_{\mathtt{f}}^{-} + \mathbf{B}\boldsymbol{\Phi}_{\mathtt{q}}^{-}\right) \quad \text{and} \quad \mathbf{r}_{\mathtt{R}} = -\left(\mathbf{A}\boldsymbol{\Phi}_{\mathtt{f}}^{-} + \mathbf{B}\boldsymbol{\Phi}_{\mathtt{q}}^{-}\right)^{-1}\left(\mathbf{A}\boldsymbol{\Phi}_{\mathtt{f}}^{+} + \mathbf{B}\boldsymbol{\Phi}_{\mathtt{q}}^{+}\right), \tag{15}$$

where the wave modes are given at the left and right boundaries, respectively. Moreover, the amplitude of the positive going wave directly generated by the point time harmonic force at the left boundary can by found by solving $\boldsymbol{\Phi}_{\mathtt{f}}^{+}\mathbf{e}^{+} = \mathbf{f}_{\mathtt{ext}}$ [80, 20].

## 3. Metamaterial beam

In this section, a periodic metastructure composed of an I-beam with attached resonators is presented in terms of its dispersion curves and transfer receptance. Then, some cases of nearly-periodic configuration are discussed in terms of their phase and amplitude changes as well as their attenuation performance, considering variability in the bending stiffness of the I-beam and in the resonators. Finally, the effects of randomness are included in terms of a random field and the statistics of the transfer receptance are discussed.

### *3.1. Periodic metamaterial*

Considering a beam with attached resonators, the coupling between the beam and resonators produces a band gap around the tuned resonance frequency [81, 82]. This configuration leads to an acoustic mode at low-frequency, where beam and resonators move in phase, and an optical mode at higher frequencies, where beam and resonators move out of phase [83]. In mass-spring-like systems such as the one in this work, local resonances are created by the natural modes of the resonators, which absorb mechanical energy and suppress the vibration at the main structure at these specific frequencies. Therefore, around the internal band gap resonance, the resonators vibrate while the structure practically does not move. Besides, a beam with locally resonant band gaps presents a negative dispersion diagram. This can be interpreted as a negative group velocity, i.e. the wave mode propagates energy in the negative direction. Note that due to the symmetry of the unit cell, a equivalent wave mode $\mu^{-}$ will propagate energy in the positive direction. This effect is not related to the periodicity by itself and can also appear in homogeneous structures. A full discussion on these interpretations can be found in [84, 85, 86].

The model studied herein consists of an I-beam with periodically attached resonators. The nominal geometric dimensions of the unit cell shown in Fig. 3 are $l_a = \Delta = 16$ mm, $l_b = 12$ mm, $l_c = 13$ mm, $l_d = 2$ mm, $l_e = 3$ mm, $l_f = 5$ mm, $l_g = 1$ mm and $l_h = 12$ mm. The global structure has 21 cells and is made of polyamide, whose nominal properties are shown in Table 1. Free boundary conditions are assumed at both ends. The resonators are attached to both sides of the web, and the additional mass due to the resonators is around 30% of the total mass of the beam.

A Timoshenko frame Spectral Element [17, 16] is used to model the resonator mass, a second one is used to model the resonator spring, Fig. 3(a). These elements have two nodes and six degrees of freedom (DOF) per node, three displacements and three rotations, which describe vertical bending, lateral bending, extension/compression and torsion dynamic effects. Two elements are used to model the I-beam, with the middle node connecting the resonator from both sides, as shown in Fig. 3(b). After the global matrix assembly and condensation of the interior nodes, a dynamic stiffness matrix is obtained, Eq. (1), and an eigenvalue problem can be set up as presented in Section 2. In the example treated here, there is no need to improve the numerical conditioning.

Table 1: Nominal mechanical properties of the polyamide I-beam and the attached resonators.

| Property | I-beam | Resonator mass | Resonator spring |
|---|---|---|---|
| Young' modulus (GPa) | 0.86 | 0.86 | 0.72 |
| Density (kg/m$^3$) | 700 | 1000 | 700 |
| Poisson coefficient | 0.39 | 0.39 | 0.39 |
| Loss factor | 0.03 | 0.03 | 0.03 |

Figure 4 shows the dispersion relations of the periodic unit cell with and without resonators. Since $2n\pi \pm \mu$, with $n$ a integer number, are also a solutions of the transfer matrix eigenproblem, only results in the range $0 \leq \Re\{\mu\} \leq \pi$,

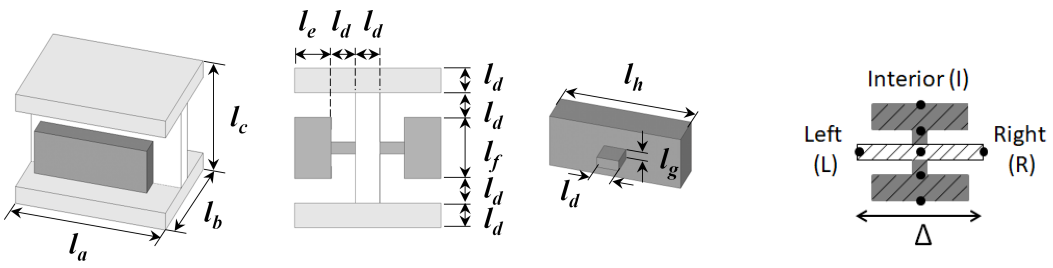


(a) (b)

Figure 3: (a) Representation of the metamaterial unit cell with cross-section view and resonator details, and (b) SE meshing with left, right and interior nodes.

i.e. the irreducible Brillouin zone, are shown. From the homogeneous beam results in Fig. 4 (a), the two vertical and lateral flexural wave modes are related to propagating (real positive part) and evanescent (imaginary negative part) waves, while the longitudinal and torsional wave modes are propagating only. For the metamaterial beam, Fig. 4 (b), it can be noticed that each wave mode has a significant imaginary component at frequencies corresponding to the stop band around the resonator frequency. This means that the corresponding waves rapidly decay, thus there is vibration attenuation in the band gap. Additionally, the flexural and torsional vibration of the resonator creates band gaps in the torsional and in the vertical flexural wave modes, also inducing vibration attenuation zones. Figure 5 presents the transfer receptance, i.e. the displacement at the right end due to a harmonic force at the left end, of the metamaterial beam. The force is applied in the vertical direction and, therefore, the displacement is only due to the vertical flexural wave mode. A notch in the response can be noticed in the frequency range predicted by the dispersion diagram of Fig. 4 (b).

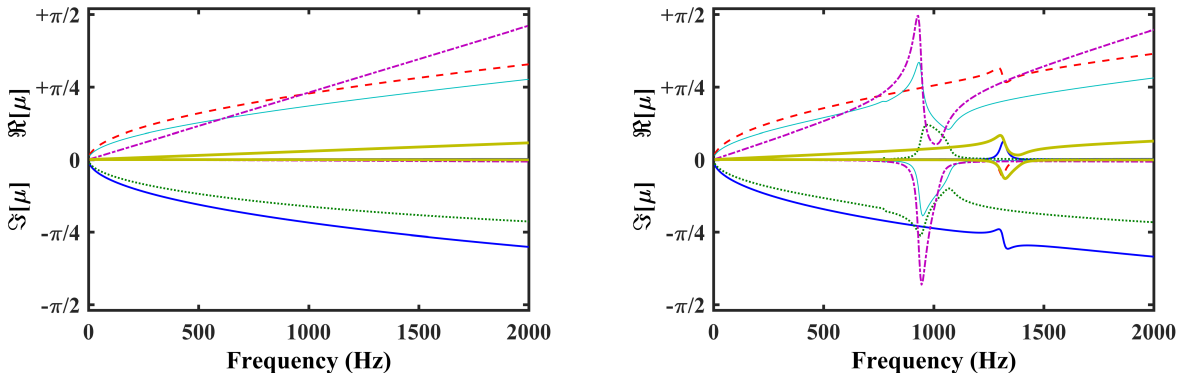


(a) (b)

Figure 4: Complex band structure for the straight beam (a) and the metamaterial beam (b), where the positive and negative values correspond, respectively, to propagating (real) and evanescent (imaginary) components of the wavenumbers related to the vertical bending 1 (cyan), vertical bending 2 (dotted green), lateral bending 1 (dashed red), lateral bending 2 (full blue), longitudinal (full yellow) and torsional (dash-dotted magenta) wave modes.

### *3.2. Nearly-periodic metamaterial*

In this section, the bending stiffness properties of the I-beam and the resonators in the metamaterial beam are considered to be varying along the beam length. Recall that they are different from the I-beam to which they are attached. First, the case of a deterministic variability is investigated and the effects of the break of periodicity of the resonators in the band gap performance are analysed. Then, the properties of the resonators are considered to be randomly varying with a spatial correlation and the statistics of the band gap performance are analysed. The latter case represents the variability of manufacturing considering an ensemble of metamaterial beams. In addition, a continuous

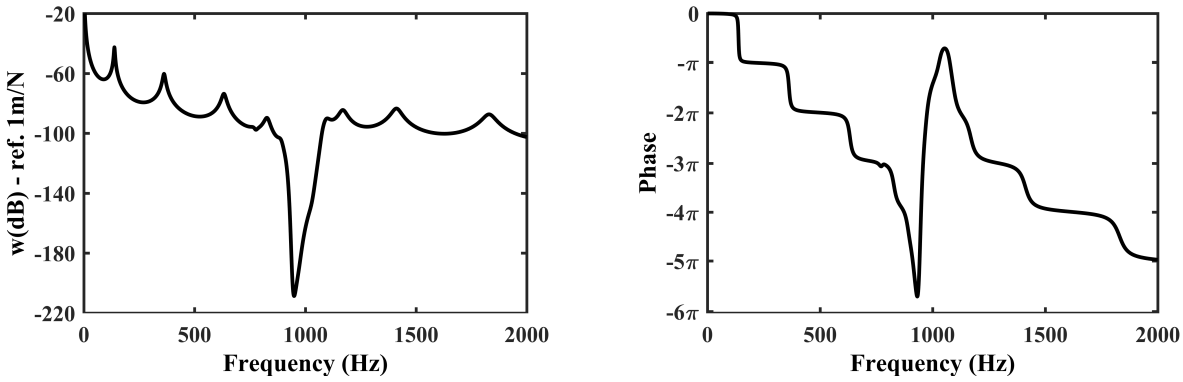


Figure 5: Amplitude and phase of the transfer receptance of the metamaterial beam in the vertical direction.

function is used to represent the spatial variability, and then the property of the cell $s$ is given by the value of the function at the centre of the cell $x_S$, i.e., the Young's modulus $E^{(s)} = E(x_s)$. This approximation holds for slowly varying properties.

### *3.2.1. Deterministic variation of the I-beam bending stiffness*

In this section, only the bending stiffness of the I-beam is considered to be spatially varying. Figure 6(a) presents the amplitude of the transfer receptance of the metamaterial beam with the flexural stiffness shown in the subplot of the same figure. The slowly varying and the full SE approaches show a very good agreement, with less than 1% error. It can be noticed that the variability in the material properties of the I-beam only affects the forced response away from the band gap region, when compared to the periodic case. Therefore, it has no direct influence on the band gap performance. This is expected, since the band gap region is only due to the resonators. Moreover, Fig. 6(b) shows the total phase change and wave attenuation of the flexural wave considered, Eq. (8), where the negative axis represents the imaginary part, i.e. the wave attenuation, and the positive axis represents the real part, i.e. the phase change. The band gap region, with significant imaginary part, is mostly unaffected.

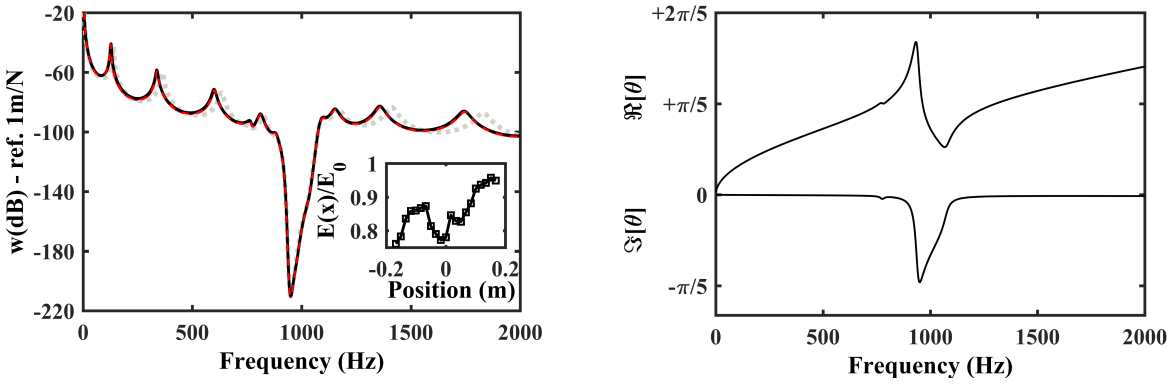


(a) (b)

Figure 6: (a) Magnitude of the transfer receptance of the metamaterial beam, periodic (dotted line) and non-periodic cases, with the slowly varying (black line) and the full SE (red line) approaches considering variable I-beam flexural stiffness (internal subplot). (b) The phase change (positive) and attenuation (negative) over the metamaterial beam length with variable I-beam flexural stiffness.

### *3.2.2. Deterministic variation of the resonators bending stiffness*

In this section, four different cases of Young's modulus spatial variability are presented, namely cases 1 to 4, represented in Fig. 7(a). Note that cases 1 and 3 have the same spatial profile, but case 3 has an increased dispersion

and cases 2 and 4 have the same spatial distribution but different dispersion. Also, the Youngs modulus of cases 2 and 4 have a smoother spatial variability than cases 1 and 3.

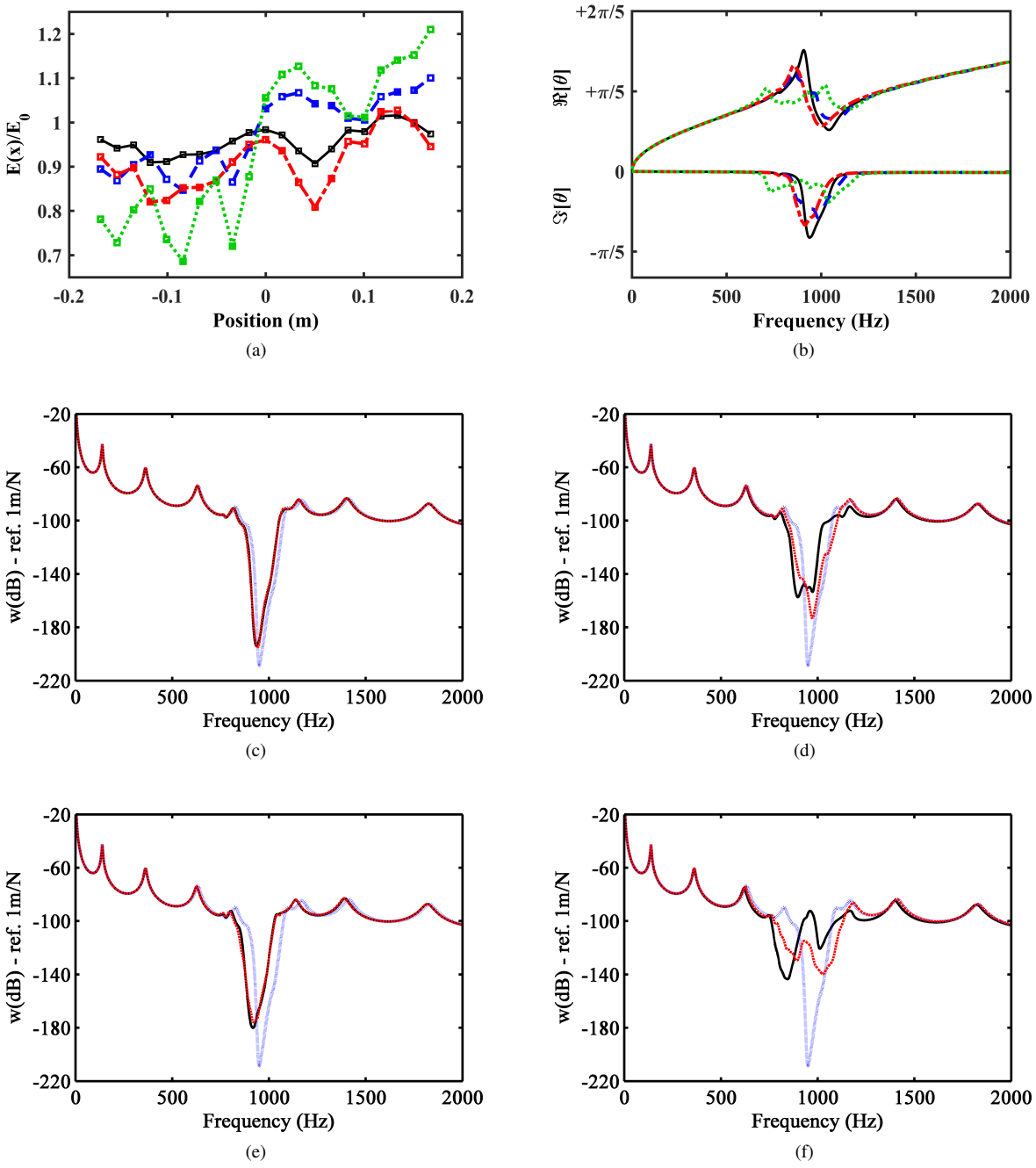


Figure 7: (a) Flexural stiffness as function of the position along the metamaterial beam and (b) phase change (positive) and attenuation (negative) over the metamaterial beam length with variable resonator flexural stiffness for case 1 (black), case 2 (blue), case 3 (red) and case 4 (green). Amplitude of the transfer receptance of the metamaterial beam with periodic (blue dotted line) and non-periodic flexural stiffness with the slowly varying approach (black line) and the full SE method (red line) for (c) case 1, (d) case 2, (e) case 3 and (f) case 4.

The forced response is calculated using the full SE method, i.e., each unit cell is given by an SE assembly with constant properties and a full dynamic stiffness matrix is constructed similarly to a standard FE procedure. The

harmonic displacements of the finite structure ($\mathbf{q}_{\mathtt{G}}(\omega)$) are computed after the assembly of the global dynamic stiffness matrix ($\mathbf{D}_{\mathtt{G}}(\omega)$) as well as by imposing harmonic external forces ($\mathbf{f}_{\mathtt{G}}(\omega)$) and boundary conditions. The assembly process can be written as $\mathbf{D}_{\mathtt{G}}(\omega) = \boldsymbol{\mathcal{A}}_{\mathtt{s}=1}^{\mathtt{N}}\mathbf{D}_{\mathtt{s}}$, where $\boldsymbol{\mathcal{A}}$ is the finite element-like assembly operator for $N$ unit cells, moreover $\mathbf{D}_{\mathtt{s}}$ is the condensed dynamic stiffness matrix of the unit cell described with SE. Therefore, the spectral displacements are achieved by solving the linear system $\mathbf{q}_{\mathtt{G}}(\omega) = \mathbf{D}_{\mathtt{G}}(\omega)^{-1}\mathbf{f}_{\mathtt{G}}(\omega)$. Additionally, the slowly varying approach, described in Section 2.2, is also used to calculate the forced response using $N_{gl} = 8$ points for all cases. Figure 7(c-f) presents the amplitude of the transfer receptance of the metamaterial beam with non-homogeneous Young's modulus as shown in Fig. 7(a). It can be seen that the slowly varying approach has a very good agreement with the full SE model, except for cases (d) and (f) in the band gap region.

It can be noticed that the band gap performance is very sensitive to the spatial variation profile and overall spatial level of dispersion. In general, a slight increase in the level of dispersion has the effect of decreasing the level of vibration suppression, while the spatial variability profile has the effect of changing the band gap width. This effect can be explained from the total phase and attenuation changes, shown in Fig. 7(b). For increasing dispersion, the change in attenuation, given by the negative axis of the figure, is smaller. However, the change in spatial variability profile affects the width of the imaginary part. Cases 2 and 4 have a larger net change of Young's modulus than cases 1 and 3. This net change has the effect of further decreasing the level of vibration suppression, but for case (f) it also generates a wider bandwidth of vibration attenuation. This variability in the Young's modulus promotes a mistuning around the designed fundamental frequency of the resonators therefore creating an effect similar to a rainbow metamaterial [62, 87]. The mismatch in the amplitude of the transfer receptance from the slowly varying approach and the full SE method, Fig.7(f) suggests that there is at the formation of at least one turning point along the beam in the attenuation frequency range, leading to wave or mode localization, as described by Luongo [59]. A critical section is created at the transition between these two regions, generating wave reflections due to the local change from cut-on/cut-off waves. This is also known as a turning point [88] and breaks the assumption of negligible reflected waves, even though the properties are slowly varying. This effect is experimentally verified described in terms of vibration amplitudes by Beli et al. [26]. Moreover, it is been known for decades that near-periodic structures and can be optimized for improved vibration attenuation [28, 89]. In this sense, the mistuning of the resonators in metastructures can also be optimized for improved attenuation performance beyond the typical periodic approach. A practical design approach has been recently proposed by Meng et al. [90] by using additive manufacturing techniques and varying some geometrical parameters of the resonators following an optimized spatial profile. Also, Cardella et al. [91] have proposed a design using an array of shunted piezoelectric patches tuned at designed frequencies to obtain a rainbow trap effect.

### *3.3. Stochastic analysis considering spatially correlated randomness*

In this section, the bending stiffness properties of resonators in the metamaterial beam are considered to be randomly varying along the beam length, with a given spatial correlation. The effects of the random field correlation length, i.e., the scale of spatial fluctuation, on the band gap performance are investigated. Random field theory has been successfully used to model spatially distributed variability in structural dynamics in the past decades [92, 52, 93], with much focus on composite structures (e.g. [94]) and increasing attention to structures produced from additive manufacturing [95], including description of spatially correlated randomness [96, 26]. The KL expansion is used to represent the random field and details are given in Appendix A.

For this analysis, the Young's modulus $E$ was chosen to be randomly varying according to a random field, i.e., $E(x) = H(x)$. Figure 8 shows the mean value, the $5^{th}$ and the $95^{th}$ percentiles of the transfer receptance of the metamaterial beam with random flexural stiffness with the slowly varying approach and the full SE method considering $\sigma = 0.1$ and four correlation length cases, namely $b = 0.25L$, $b = 0.5L$, $b = 0.75L$ and $b = L$. These statistics were obtained from 1000 Monte Carlo (MC) samples. The result from the periodic case is also plotted for comparison. It is noticeable that the slowly varying approach is able to accurately represent the response percentiles and mean value, even with some specific sample presenting critical sections. Moreover, it can be seen that the correlation length plays a role on the uncertainty bounds of the response. Larger random field correlation lengths create smoother spatial variability with a bigger net change, as can be seen from Fig. 8, which shows random field samples with a large correlation length. As discussed in Section 3.2.2, this effect tends to widen the band gap and also decrease the level of vibration attenuation, which, over the ensemble of metamaterial beams, pushes the $95^{th}$ percentile to upper bounds, as shown in more detail in Fig. 9(a). Finally, the $5^{th}$ and $95^{th}$ percentiles of the vertical flexural attenuation and phase change

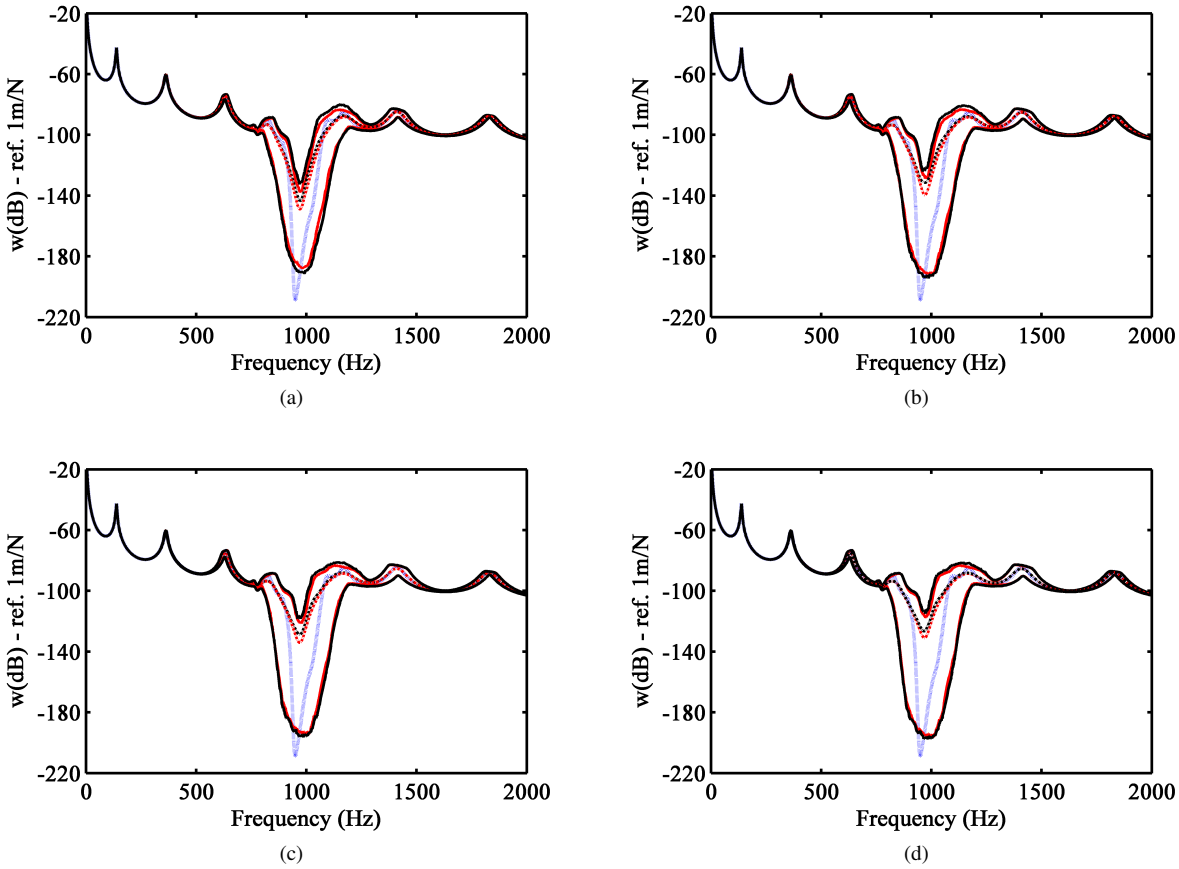


Figure 8: The mean value, $5^{th}$ and $95^{th}$ percentile of the amplitude of the transfer receptance of the metamaterial beam with random flexural stiffness with the slowly varying approach (black line) and the full SE method (red line) with $\sigma = 1$ and correlation length (a) $b = 0.25L$, (b) $b = 0.5L$, (c) $b = 0.75L$ and (d) $b = L$, and also the periodic case (blue dotted line).

are shown in Fig. 9(b-c). It can be seen that the variability of the resonators affects only the band gap region and also that the attenuation band increases for increasing correlation lengths, which explains the results presented in Fig. 8. Even though it might not be representative for some of the individual samples with turning points, as seen in Fig. 7(a), it represents the overall tendency of the ensemble.

## 4. The phononic undulating beam

In this section, a phononic crystal structure composed of an undulating beam is presented in terms of its dispersion curves and transfer receptance. A similar analysis to the previous case is presented and the differences on the performance of the phononic crystal with respect to the metastructure are highlighted. Moreover, in this section, the unit cell is based on a FE model of a continuously varying structure, hence, the slowly varying WFE approach previously proposed [51] is used. The main difference is that this assumes a locally defined wavenumber and then Eqs. (8) and (10) are modified accordingly.

### *4.1. Uniform phononic crystal*

In this work, undulating beams are periodic structures where the beam neutral axis presents an orthogonal undulation given by $\mathsf{c}(x) = c_0 \cos(2\pi x/\Delta)$, where $c_0$ is the amplitude and $\Delta$ the unit cell length. The unit cell schematic as well as its FE meshing are shown in Fig. 10. The coupling between flexural and longitudinal waves produces the

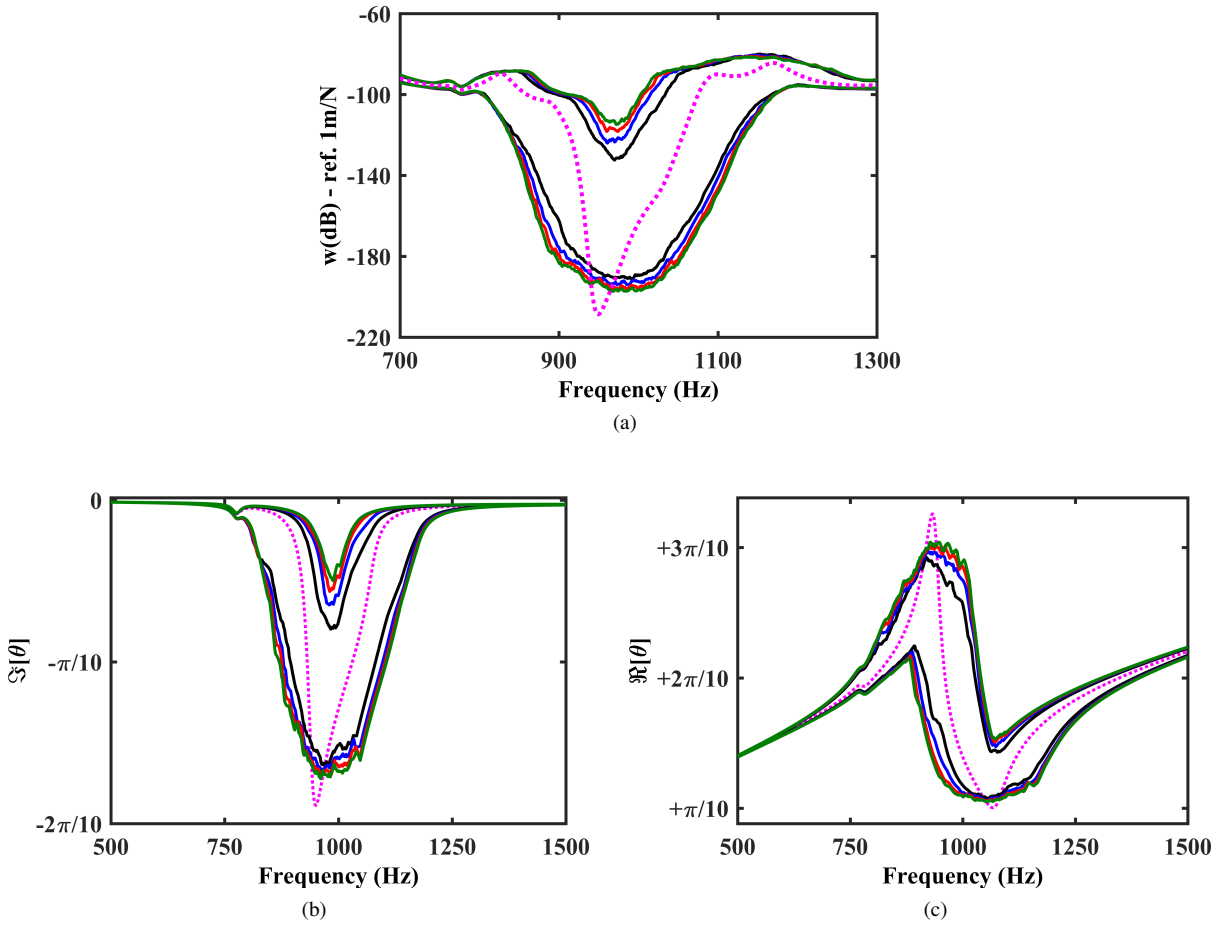


Figure 9: Detail of the $5^{th}$ and $95^{th}$ percentile of the amplitude of the transfer receptance (a), attenuation change ($\Im[\mu]$) (b) and phase change ($\Re[\mu]$) (c) of the metamaterial beam with slowly varying flexural stiffness in the resonators, b = 0.25L (black line), b = 0.50L (blue line), b = 0.75 L (red line) and b = 1L (green line) and periodic case (magenta dotted line).

band gaps. Moreover, an Euler-Bernoulli model has been used to demonstrate that the beam thickness and the beam undulation are responsible, respectively, for the location and width of the phononic band gaps [67].

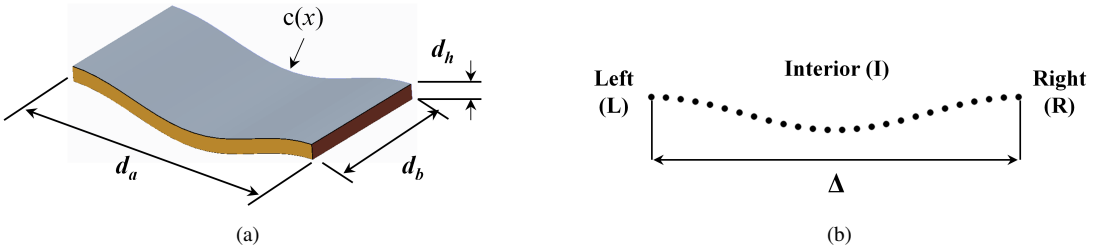


Figure 10: (a) Representation of the phononic unit cell, and (b) FE meshing with left, right and interior nodes.

Assuming harmonic motion, the governing equation of a unit cell modelled using FE is written as $\widetilde{\mathbf{D}}\hat{\mathbf{q}} = \hat{\mathbf{f}}$, where by $\widetilde{\mathbf{D}} = \mathbf{K} - \omega^2\mathbf{M}$ is the dynamic stiffness matrix, $\mathbf{M}$ is the mass matrix, $\mathbf{K}$ is the stiffness matrix and $\omega$ is the angular frequency. In this case, these matrices are extracted from the software Ansys® and the mesh contains at least 8 elements per wavelength in order to appropriately represent numerically the wave behaviour. Timoshenko beam

element BEAM188 with two nodes and six degrees of freedom per node is used. In addition, the structural damping, $\eta$, is modelled as a complex term of the stiffness matrix, $\mathbf{K} = \mathbf{K}(1 + \mathtt{i}\eta)$. This FE model has two main differences when compared to Euler-Bernoulli analytic equations [67]: it takes into account the Poisson's ratio and out of plane behaviour. It is assumed that the beam is made of nylon, such that $E = 1$ GPa, $\rho = 1000$ kg/m$^3$, $\nu = 0.3$ and $\eta = 0.02$ while the nominal values of the geometric parameters are $d_a = \Delta = 25$ mm, $d_h = 2.5$ mm, $d_b = 12.5$ mm and the undulating amplitude to cell length ratio $\xi = c_0/\Delta = 0.025$. These nominal values are used for the band structure, i.e. the dispersion diagram, and forced response calculation in the periodic case.

The dispersion curves for both straight and undulating beams are shown in Fig. 11. Six branches are observed, due to vertical and lateral bending, longitudinal, and torsional waves. Note that below 2 kHz the effects of the undulating are negligible and both dispersion curves are identical. The longitudinal-vertical bending wave coupling is responsible for opening one band gap around 5100 Hz, another band gap also opens almost in the same frequency range due to torsional-lateral bending wave coupling. In addition, partial band gaps due to Bragg scattering occur for the vertical bending and torsional waves at the Bragg limits $\Re[\mu] = \{0 \text{ or } \pi\}$, due to the spatial periodicity. Each corresponding band gap can also be distinguished by the imaginary part of the wavenumbers, which correspond to wave attenuation, and where $\Im[\mu]$ has a semicircular shape. In the stop band regions, two distinct real solutions merge to form a complex conjugate pair, which is also known as wave locking [76], and couples both wave types.

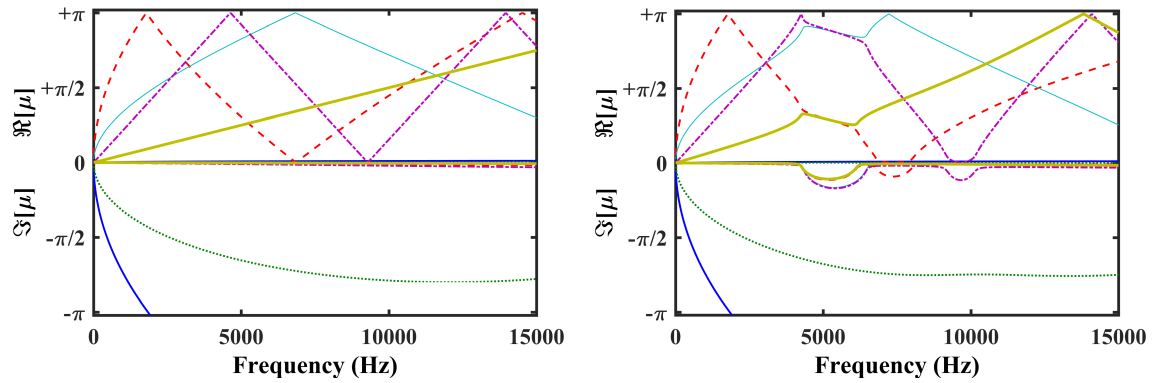


Figure 11: Complex dispersion structure for the straight beam (a) and undulating beam (b), where the positive and negative values correspond, respectively, to propagating (real) and evanescent (imaginary) components of the wavenumbers. Wavenumbers corresponding to vertical bending 1 (dashed red), vertical bending 2 (full blue), lateral bending 1 (full cyan), lateral bending 2 (dotted green), longitudinal (full yellow) and torsional (dash-dotted magenta) waves.

The amplitude and phase of the transfer receptance, i.e. a point harmonic transverse force is applied at one end and the transverse displacement is found at the other end, for the periodic undulated beam with $N = 20$ is presented in Fig. 12. Free-free boundary conditions are assumed. Clearly, a vibration attenuation zone with a constant phase is observed around 5100 Hz, which characterizes the band gap due to wave locking. However, the partial band gap of the vertical bending wave at 7300 Hz doesn't attenuate the vibration. In addition, amplified resonance vibration peaks appear at the lower and upper boundaries of the attenuation zone, which impair the band gap performance.

### *4.2. Nearly-periodic phononic crystal*

In this section, the material and geometric properties of the undulating beam are considered to be slowly varying along its length. As presented in Appendix A, the spatial profile of the properties is represented by a continuous function, and the unit cell properties are assumed constant with value given by the centre of the cell, i.e, $\zeta^s = \zeta(\bar{x}_s)$, where $s$ is the unit cell number, $\bar{x}_s$ is the unit cell centre position and $\zeta(x)$ is the continuous function for the material (e.g., elastic modulus) or geometric (e.g., beam height) properties. The $\zeta(x)$ functions are given by the KL expansion, and the effects of breaking the translational periodicity on the phase change of a wave propagating along the beam and forced response of the finite phononic crystal using $N_{gl} = 8$ integration points are investigated. Moreover, the

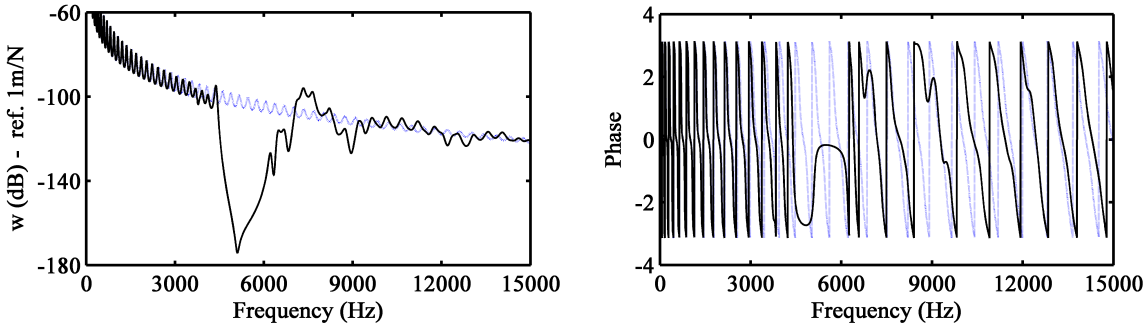


(a) (b)

Figure 12: Amplitude (a) and phase (b) of the transfer receptance of the periodic undulated beam (black full line) and straight beam (blue dotted).

limitations of the slowly varying formulation will be discussed by investigating the critical sections where its main assumptions are no longer valid. Here, the phononic beams are analysed individually.

First, a sensitivity analysis is performed by varying the elastic modulus along the beam length for different standard deviations, or dispersion amplitudes, as shown in Fig. 13(a). The corresponding phase and attenuation changes for the vertical flexural wave at the band gap zone are presented in Fig. 13(b-c). In addition, the forced responses from the full FE and the slowly varying WFE approaches are shown in Fig. 13(d-f), respectively. It can be observed that the higher the standard deviation or the net change, the more intense is the "jagged" profile inside the band gap, and the smaller the vibration attenuation bandwidth for the same intensity reduction. In addition, the response from the slowly varying approach gets progressively more distant from the reference full FE solution. This is more noticeable for case 3, especially at the lower and upper band gap boundaries, which are related to the transition between the attenuation-propagation zones due to the wave locking, and hence, to the critical sections. This issue is captured by undulations in the flexural vertical phase and amplitude changes, which smooths out the transition. Note that the response is in agreement to the FE results in the other frequency regions which shows for this case that the discrepancies are strictly related to the turning points created by the spatially varying band gaps.

A similar analysis is performed on the beam thickness by varying it along the beam length, with the same spatial profiles, as shown in Fig. 14(a). The phase and amplitude change for the vertical flexural wave are presented in Fig. 14(b) and Fig. 14(c), respectively, in the band gap frequency region. In addition, the amplitude of each corresponding forced response is shown in Fig. 14(d-f). Note that the dynamic behaviour is more sensitive to the geometric variation than to the material variation, i.e., for the same distribution profiles, the phase and amplitude change are more affected, which can be observed by the undulating profile in the imaginary part of the wavenumber. In addition, the attenuation performance profile is modified by increasing the standard deviation and consequently gives the "jagged" appearance of the forced response. Moreover, unlike the previous analysis, the attenuation bandwidth increases when compared to the periodic case. Finally, it can be noticed that the critical sections are formed at lower net change such that the forced response starts to diverge from the full FE solution at smaller values of the standard deviation, e.g. in case 2.

### *4.3. Stochastic analysis considering spatially correlated randomness*

In this section, the random field formulation from the previous subsection (presented in Appendix A) is used and the properties as well as the dynamic response are investigated from the ensemble statistics estimated from a MC sampling. Based upon the previous investigations, both material and geometric parameters are important and will be taken in account in the stochastic analysis. Moreover, the effects of the random field correlation length, i.e., the length scale of spatial fluctuation, on the band gap performance are investigated. The random field distributions ($H(x) = \{E(x)$ or $h(x)\}$) are generated from the KL expansion for a given correlation length and standard deviation, the forced response is computed for each sample, and the statistics estimated. Hence, the attenuation performance can be stochastically analysed.

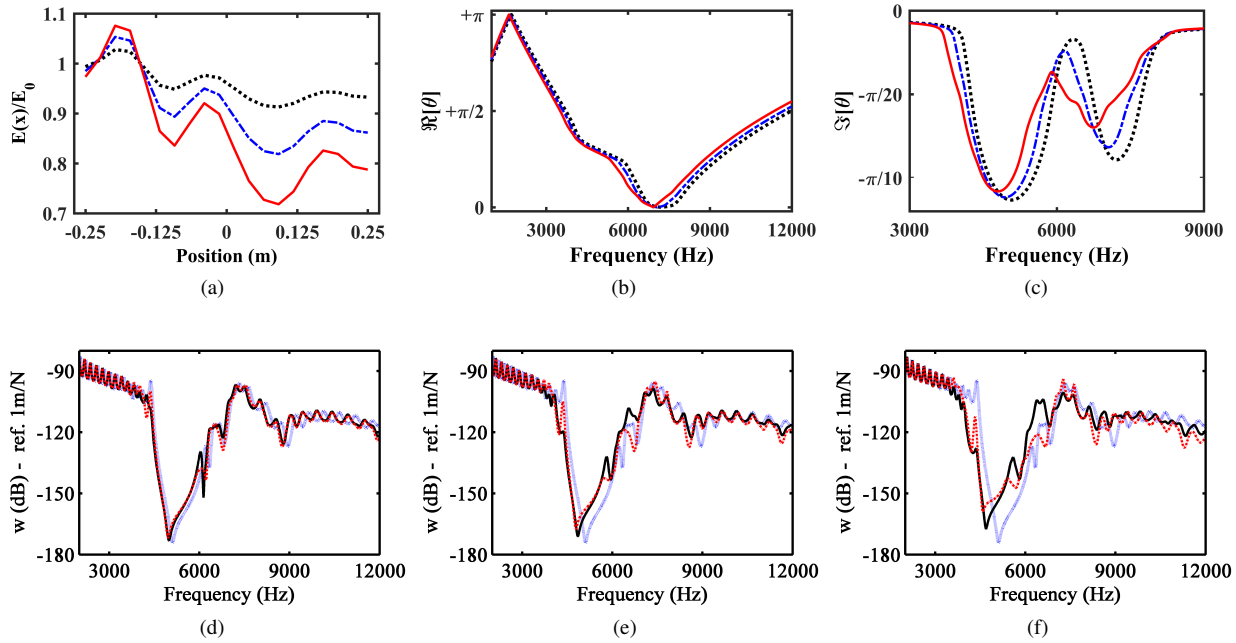


Figure 13: Deterministic variation of elastic modulus (a), and real (b) and (c) imaginary components of the phase change, legend: case 1 (black), case 2 (blue) and case 3 (red). Dynamic response for the case 1 (c), case 2 (e) and case 3 (f), legend: slowly varying approach (red), full FE model (black) and periodic undulating beam (blue).

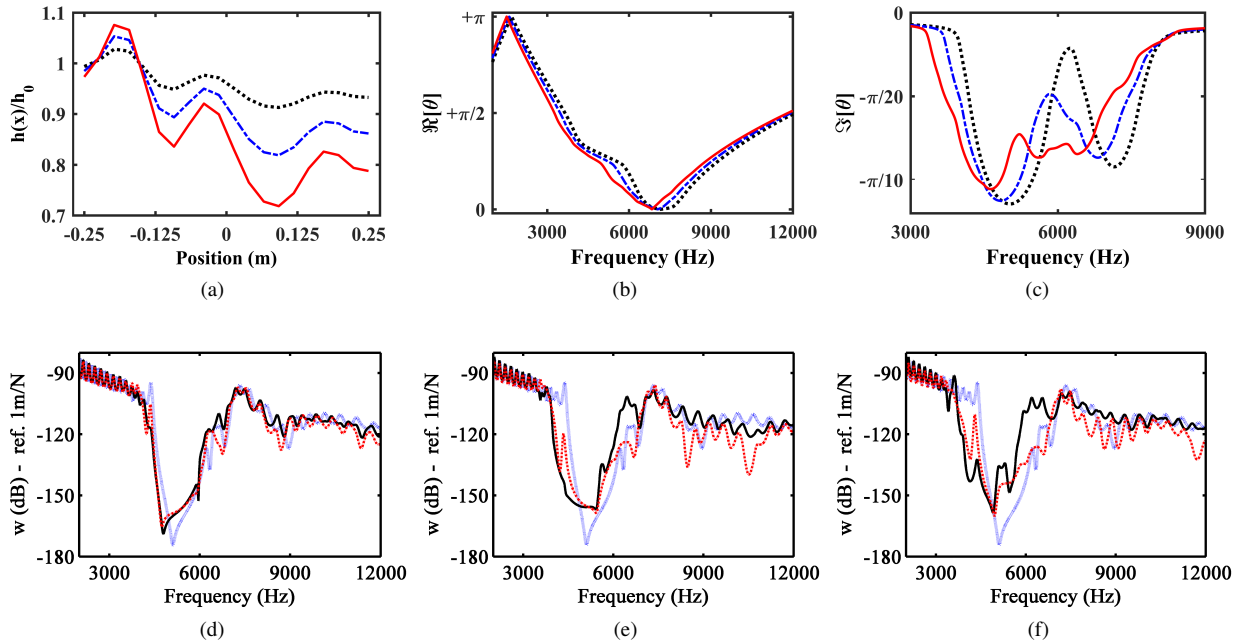


Figure 14: Deterministic variation of beam thickness (a), and real (b) and (c) imaginary components of the phase change, legend: case 1 (black), case 2 (blue) and case 3 (red). Dynamic response for the case 1 (c), case 2 (e) and case 3 (f), legend: slowly varying approach (red), full FE model (black) and periodic undulated beam (blue).

The mean value, $5^{th}$ and $95^{th}$ percentiles of the dynamic response are shown in Fig. 15 for the same random field standard deviation and two correlation lengths $b = 0.25L$ and $b = 1L$, calculated from the full FE model and the proposed slowly varying WFE approach. The slowly varying approach presents a good agreement of the mean value and percentile envelope when compared to the full FE solution in all of the frequency range, except at the limits of the band gap for the case of varying Young's modulus, 15(a-b). However, for the case of varying thickness, only the mean value has a good agreement with the full FE solution for frequencies higher than the band gap, 15(c-d). In addition, it can be noticed that the overall response envelope is mostly unaffected by the correlation length apart from the band gap region. This is expected due to the high modal density of the structure. For the same standard deviation, the percentiles in the band gap region increase for increasing correlation length, showing that the spatial profile also plays a role on the ensemble performance of the vibration attenuation. This is very important for robustness and shows that neglecting the spatial correlation on the stochastic analysis of band gaps might be misleading (e.g. [37, 97]).

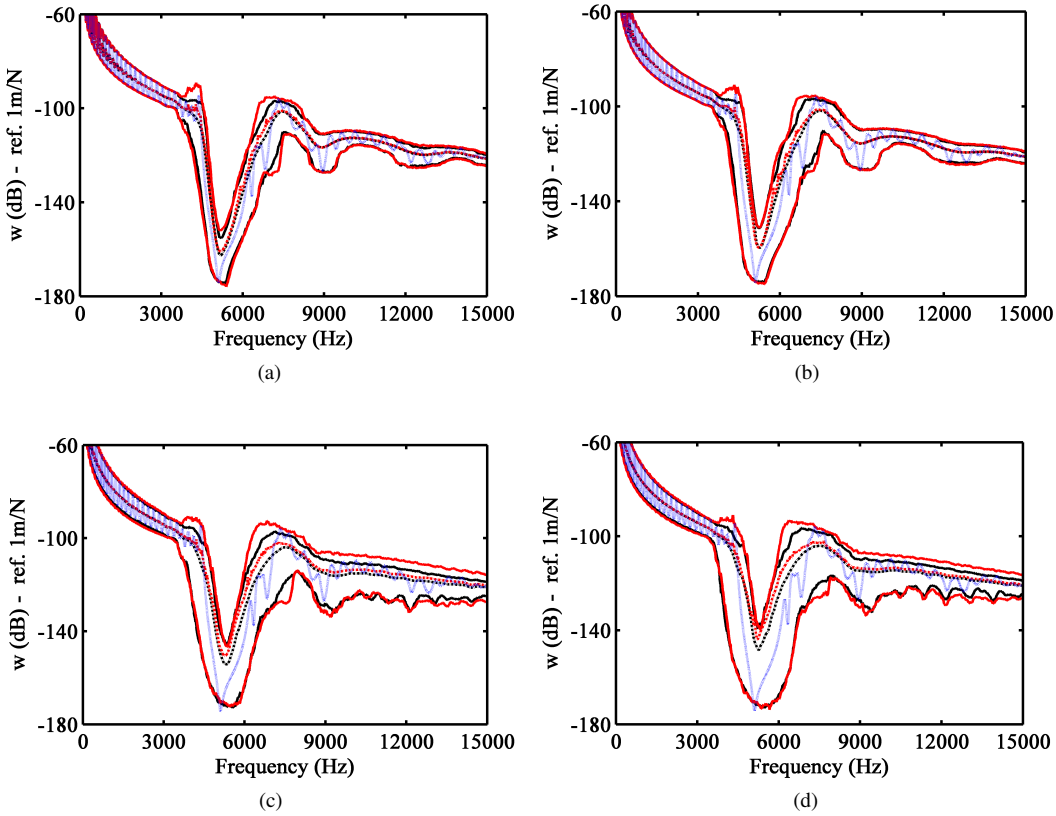


Figure 15: The mean value, $5^{th}$ and $95^{th}$ percentile of the amplitude of the transfer receptance of the undulating beam with random elastic modulus (a, b) and beam thickness (c, d) with the slowly varying approach (black line) and the full FE method (red line) considering $\sigma = 0.10$ and (a) $b = 0.25L$, (b) $b = 1L$, (c) $b = 0.25L$ and (d) $b = 1L$, and also the periodic case (blue dotted line).

Finally, parametric analysis of the transfer receptance and phase attenuation by varying the correlation length are shown in Fig. 16(a-b) and Fig. 16(c-d), respectively. For a fixed value of $\sigma = 0.10$, the area covered by the $5^{th}$ and $95^{th}$ percentiles (i.e., the variability of the response) is larger for higher correlation lengths. Therefore, the higher the variability, the broader the attenuation vibration zone which increases with the correlation length. Because the dynamic response is more sensitive to thickness than to elastic modulus, the confidence bounds are wider for the latter parameter. By analysing the $5^{th}$ and $95^{th}$ percentiles of the vertical flexural attenuation change in Fig. 16(c-d), for both parameters the band gap due to the wave coupling is robust to variability because a significant imaginary component is presented. On the other hand, the partial band gap due to Bragg scattering is more sensitive and hence it is not robust to the variability. The corresponding phase and attenuation changes are plotted in Fig. 16(e-f). For elastic

modulus variation, the $5^{th}$ and $95^{th}$ percentiles (i.e., the net change) proportionally increase in frequency without relation to the band gap. However, for the thickness variation, the $5^{th}$ and $95^{th}$ percentiles increase at the band gaps without relation to the excitation frequency.

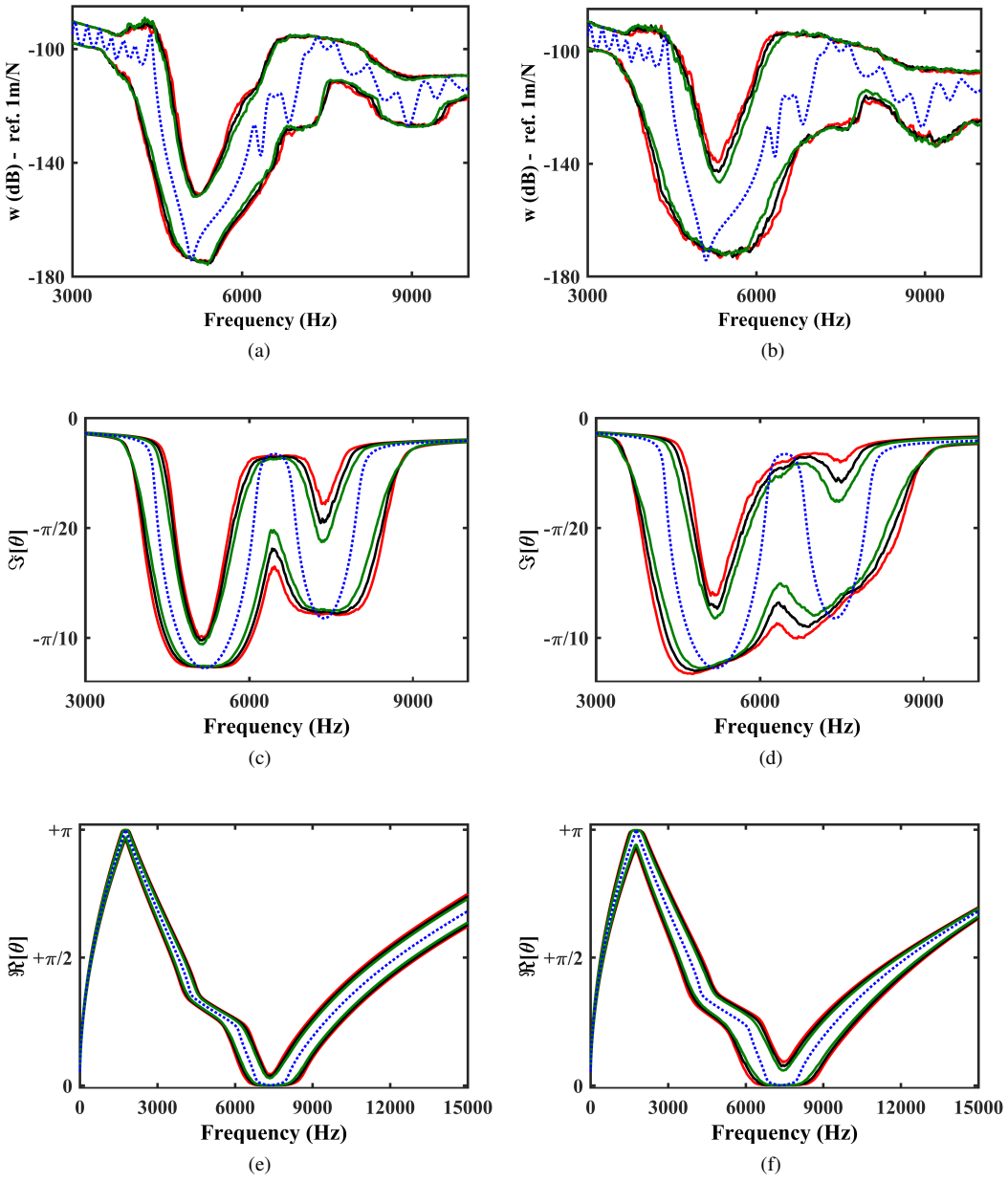


Figure 16: Detail of the $5^{th}$ and $95^{th}$ percentile of the amplitude of the transfer receptance (a-b), and attenuation change ($\Im[\mu]$) (c-d) and phase change ($\Re[\mu]$) (e-f) of the vertical flexural wave with slowly varying elastic modulus (a, c, e) and beam thickness (b, d, f), legend: b = 0.25L (red line), b = 0.50L (black line), b = 1L (green line) and periodic case (blue dotted line).

## 5. Concluding remarks

In this work, the effects of spatially correlated material and geometrical variability on the band gap of metamaterials and phononic crystals were analysed using a slowly varying approach. It was seen that the spatial profile of the variability plays an important role on the vibration attenuation performance. The analysis of the phase and attenuation change over the length of a beam shows the presence of critical sections, known as turning points in the WKB context, which can drastically change the frequency bandwidth and maximum attenuation of the band gap. A critical section is created in the transition between zones of propagating and non-propagating waves at a given frequency and they typically appear in a band around cut-on/cut-off frequencies and at the edges of wave locking and veering.

Although the slowly varying approach is not an accurate representation of the response in the presence of critical sections, due to the consequent wave reflections, it is still possible to investigate the vibration attenuation performance with the phase and attenuation change analysis. Moreover, it can also capture the ensemble statistics of metamaterials and phononic crystals, providing a suitable framework for uncertainty analysis.


## Acknowledgements

The authors also grateful to the São Paulo Research Foundation (FAPESP - São Paulo, Brazil), through project numbers 2014/19054-6 and 2018/15894-0, Brazilian National Council of Research (CNPq - Brazil), processes number 420304/2018-5 and 231744/2013-7, the Federal District Research Foundation (FAPDF - Distrito Federal, Brazil), process number 0193.001507/2017 and the Coordination for the Improvement of Higher Education Personnel (CAPES - Brazil) for the financial support.


## Appendix A. Karhunen-Loève expansion

A random field $H(x,p)$ can be defined as a collection of random variables indexed by a continuous parameter $x \in D$, where D describes the system domain. In other words, for a given position $x_0$, $H(x_0,p)$ is a random variable, and for a given outcome $p$, $H(x,p)$ is a realization of the field. Amongst the methods available in the literature for generating random fields (e.g. [98]), the KL expansion is a special case of series expansion using random variables and deterministic spatial functions which are orthogonal and derived from the covariance function. A homogeneous random field with a finite, symmetric and positive definite covariance function, defined over a domain, has a spectral decomposition in the generalized series [52]

$$H(x) = H_0 + \sum_{j=1}^{\infty} \sqrt{l_j} X_j f_j(x) \tag{A.1}$$

where $H_0$ is the random field mean value, $X_j$ are uncorrelated random variables, $l_j$ and $f_j(x)$ are eigenvalues and eigenfunctions, solutions of the Fredholm integral equation of the second kind from the covariance function [52] and the $p$ dependence has been omitted.

The eigenvalues and eigenfunctions can be ordered in descending order of magnitude of the eigenvalues to truncate the series in Eq. (A.1) to a finite number of terms $N_{\mathrm{KL}}$, chosen by the accuracy of the series in representing the covariance function, rather than the number of random variables [78]. As a rule of thumb, $N_{\mathrm{KL}}$ can be chosen such that $l_j/l_1 < 0.1$, and it depends on the correlation length of the random field. The longer the correlation length the more rapidly the eigenvalues decrease, meaning that fewer terms are needed to accurately represent the series.

If $H(x)$ is a Gaussian random field, $X_j$ are always independent zero mean unit standard deviation Gaussian random variables. However, if the random field is not Gaussian it is not possible to use the KL expansion to directly generate a $H(x)$ because $X_j$ have unknown joint PDF. Some approaches have been proposed to overcome this issue, amongst them an iterative scheme [99, 100], which uses directly the KL expansion and can simulate both stationary and non-stationary random fields. Moreover, if the target CDF is approximately Gaussian, only one iteration might be enough to achieve convergence. In general, the eigenproblem can only be solved numerically and normally involves some procedure for discretizing the random field [101, 98]. However, for some families of correlation functions and specific geometries, there exist analytical solutions of this integral equation [52].

The Latin Hypercube sampling (LHS) can be used as a stochastic solver and has the advantage of being as general as the classical Monte Carlo (MC) solver, in which given the probability measure of the random variables several samples are generated and the statistic of the response can be evaluated, but with increased computational efficiency due to the reduction of the required number of realizations for convergence. For the Monte Carlos analysis, the beam properties ($\beta$) was chosen to be randomly varying according to a random field, i.e., $\beta(x) = H(x)$, where $H(x)$ is a Gamma distributed homogeneous random field with correlation function given by

$$C(\tau) = e^{-|\tau|/b}, \tag{A.2}$$

where $\tau$ is lag or the distance between any two points in the random field, $b$ is the correlation length. Then, an analytical solution for Eq. (A.1) is available [52]. The properties within each cell are specified to be constant and given by $H(x_c)$, where $x_c$ is the centre of each cell. This approximation is accurate for large correlation lengths [102].

The Gamma distribution is chosen to model the stochastic Young's modulus because it is defined for strictly positive values. It is given by

$$f_\beta(x) = \frac{x^{a_0-1}e^{-x/b_0}}{b_0^{a_0}\Gamma(a_0)}, \quad x > 0, \tag{A.3}$$

where $\Gamma(x) = \int_0^{+\infty} t^{x-1}e^{-t}dt$, $x > 0$ is the Gamma function and the parameters of the distribution are given by $a_0 = 1/\delta_\beta^2$ and $b_0 = \beta_0\delta_\beta^2$, where $\delta_\beta$ is the dispersion parameter and $\beta_0$ is the mean value. Equation (A.1) is used to simulate the non-Gaussian random field [99, 100] and the LHS scheme is used as a stochastic solver [103, 104].

## References


[1] M.-H. Lu, L. Feng, Y.-F. Chen, Phononic crystals and acoustic metamaterials, Materials Today 12 (12) (2009) 34 – 42. doi:10.1016/S1369-7021(09)70315-3.

[2] M. Maldovan, Sound and heat revolutions in phononics, Nature 503 (2013) 209. doi:10.1038/nature12608.

[3] M. I. Hussein, M. J. Leamy, M. Ruzzene, Dynamics of phononic materials and structures: Historical origins, recent progress, and future outlook, Applied Mechanics Reviews 66 (4) (2014) 040802–040802–38. doi:10.1115/1.4026911.

[4] G. Ma, P. Sheng, Acoustic metamaterials: From local resonances to broad horizons, Science Advances 2 (2) (2016) e1501595. doi:10.1126/sciadv.1501595.

[5] H. H. Huang, C. T. Sun, Wave attenuation mechanism in an acoustic metamaterial with negative effective mass density, New Journal of Physics 11 (1) (2009) 013003. doi:10.1088/1367-2630/11/1/013003.

[6] E. Baravelli, M. Ruzzene, Internally resonating lattices for bandgap generation and low-frequency vibration control, Journal of Sound and Vibration 332 (25) (2013) 6562 – 6579. doi:10.1016/j.jsv.2013.08.014.

[7] Z. Yang, H. M. Dai, N. H. Chan, G. C. Ma, P. Sheng, Acoustic metamaterial panels for sound attenuation in the 50–1000 hz regime, Applied Physics Letters 96 (4) (2010) 041906. doi:10.1063/1.3299007.

[8] C. Claeys, E. Deckers, B. Pluymers, W. Desmet, A lightweight vibro-acoustic metamaterial demonstrator: Numerical and experimental investigation, Mechanical Systems and Signal Processing 70-71 (Supplement C) (2016) 853 – 880. doi:10.1016/j.ymssp.2015.08.029.

[9] S. A. Cummer, D. Schurig, One path to acoustic cloaking, New Journal of Physics 9 (3) (2007) 45. doi:10.1088/1367-2630/9/3/045.

[10] S.-C. S. Lin, T. J. Huang, J.-H. Sun, T.-T. Wu, Gradient-index phononic crystals, Phys. Rev. B 79 (2009) 094302. doi:10.1103/PhysRevB.79.094302.

[11] S. H. Mousavi, A. B. Khanikaev, Z. Wang, Topologically protected elastic waves in phononic metamaterials, Nature Communications 6 (2015) 8682. doi:10.1038/ncomms9682.

[12] R. K. Pal, M. Ruzzene, Edge waves in plates with resonators: an elastic analogue of the quantum valley hall effect, New Journal of Physics 19 (2) (2017) 025001. doi:10.1088/1367-2630/aa56a2.

[13] O. Sigmund, J. Søndergaard Jensen, Systematic design of phononic band–gap materials and structures by topology optimization, Philosophical Transactions of the Royal Society of London A: Mathematical, Physical and Engineering Sciences 361 (1806) (2003) 1001–1019. doi:10.1098/rsta.2003.1177.

[14] M. Sigalas, E. Economou, Elastic and acoustic wave band structure, Journal of Sound and Vibration 158 (2) (1992) 377 – 382. doi:10.1016/0022-460X(92)90059-7.

[15] Z. Liu, X. Zhang, Y. Mao, Y. Y. Zhu, Z. Yang, C. T. Chan, P. Sheng, Locally resonant sonic materials, Science 289 (5485) (2000) 1734–1736. doi:10.1126/science.289.5485.1734.

[16] J. Doyle, Wave Propagation in Structures: Spectral Analysis Using Fast Discrete Fourier Transforms, Mechanical Engineering Series, Springer New York, 1997.

[17] U. Lee, Spectral Element Method in Structural Dynamics, Wiley, 2009.

[18] B. R. Mace, D. Duhamel, M. J. Brennan, L. Hinke, Finite element prediction of wave motion in structural waveguides, The Journal of the Acoustical Society of America 117 (5) (2005) 2835–2843. doi:10.1121/1.1887126.

[19] J. M. Mencik, M. N. Ichchou, Multi-mode propagation and diffusion in structures through finite elements, European Journal of Mechanics - A/Solids 24 (5) (2005) 877–898. doi:10.1016/j.euromechsol.2005.05.004.

[20] J. M. Renno, B. R. Mace, On the forced response of waveguides using the wave and finite element method, Journal of Sound and Vibration 329 (2010) 5474–5488, 26. doi:10.1016/j.jsv.2010.07.009.
[21] J.-M. Mencik, New advances in the forced response computation of periodic structures using the wave finite element (WFE) method, Computational Mechanics 54 (3) (2014) 789–801. doi:10.1007/s00466-014-1033-1.
[22] J. M. Mencik, D. Duhamel, A wave-based model reduction technique for the description of the dynamic behavior of periodic structures involving arbitrary-shaped substructures and large-sized finite element models, Finite Elements in Analysis and Design 101 (2015) 1–14. doi:10.1016/j.finel.2015.03.003.
[23] S. A. Cummer, J. Christensen, A. Alù, Controlling sound with acoustic metamaterials, Nature Reviews Materials 1 (16001) (2016) 13. doi:10.1038/natrevmats.2016.1.
[24] R. Hague, I. Campbell, P. Dickens, Implications on design of rapid manufacturing, Proceedings of the Institution of Mechanical Engineers, Part C: Journal of Mechanical Engineering Science 217 (1) (2003) 25–30. doi:10.1243/095440603762554587.
[25] R. Goodridge, C. Tuck, R. Hague, Laser sintering of polyamides and other polymers, Progress in Materials Science 57 (2) (2012) 229 – 267. doi:10.1016/j.pmatsci.2011.04.001.
[26] D. Beli, A. T. Fabro, M. Ruzzene, J. R. F. Arruda, Wave attenuation and trapping in 3d printed cantilever-in-mass metamaterials with spatially correlated variability, Scientific Reports 9 (1) (2019) 5617. doi:10.1038/s41598-019-41999-0.
[27] C. H. Hodges, Confinement of vibration by structural irregularity, Journal of Sound and Vibration 82 (1982) 411–424, 3.
[28] R. S. Langley, Wave Transmission Through One-Dimensional Near Periodic Structures: Optimum and Random Disorder, Journal of Sound and Vibration 188 (1995) 717–743, 5. doi:10.1006/jsvi.1995.0620.
[29] C. H. Hodges, J. Woodhouse, Confinement of vibration by one-dimensional disorder, I: Theory of ensemble averaging, Journal of Sound and Vibration 130 (1989) 237–251, 2.
[30] C. H. Hodges, J. Woodhouse, Vibration isolation from irregularity in a nearly periodic structure: Theory and measurements, The Journal of the Acoustical Society of America 74 (1983) 894–905, 3.
[31] Z. C. He, J. Y. Hu, E. Li, An uncertainty model of acoustic metamaterials with random parameters, Computational Mechanics 62 (5) (2018) 1023–1036. doi:10.1007/s00466-018-1548-y.
[32] Y. Wu, X. Y. Lin, H. X. Jiang, A. G. Cheng, Finite Element Analysis of the Uncertainty of Physical Response of Acoustic Metamaterials with Interval Parameters, International Journal of Computational Methods (jun 2019). doi:10.1142/S021987621950052X.
[33] H. Al Ba'Ba'A, S. Nandi, T. Singh, M. Nouh, Uncertainty quantification of tunable elastic metamaterials using polynomial chaos, Journal of Applied Physics 127 (1) (2020) 015102. arXiv:1909.07883, doi:10.1063/1.5130685.
URL http://aip.scitation.org/doi/10.1063/1.5130685
[34] M. R. Souza, D. Beli, N. S. Ferguson, J. R. José, A. T. Fabro, A Bayesian approach for wavenumber identification of metamaterial beams possessing variability, Mechanical Systems and Signal Processing 135 (2020) 106437. doi:10.1016/j.ymssp.2019.106437.
URL http://www.sciencedirect.com/science/article/pii/S0888327019306582
[35] Z. Jia, Y. Chen, H. Yang, L. Wang, Designing Phononic Crystals with Wide and Robust Band Gaps, Physical Review Applied 9 (4) (2018) 044021. doi:10.1103/PhysRevApplied.9.044021.
[36] Y. Achaoui, V. Laude, S. Benchabane, A. Khelif, Local resonances in phononic crystals and in random arrangements of pillars on a surface, Journal of Applied Physics 114 (10) (2013) 104503. doi:10.1063/1.4820928.
URL http://aip.scitation.org/doi/10.1063/1.4820928
[37] C. Sugino, Y. Xia, S. Leadenham, M. Ruzzene, A. Erturk, A general theory for bandgap estimation in locally resonant metastructures, Journal of Sound and Vibration 406 (Supplement C) (2017) 104–123. doi:10.1016/j.jsv.2017.06.004.
[38] P. Celli, B. Yousefzadeh, C. Daraio, S. Gonella, Bandgap widening by disorder in rainbow metamaterials, Applied Physics Letters 114 (9) (2019) 91903. doi:10.1063/1.5081916.
URL https://aip.scitation.org/doi/abs/10.1063/1.5081916
[39] H. Jeffreys, On certain approximate solutions of lineae differential equations of the second order, Proceedings of the London Mathematical Society s2-23 (1) (1925) 428–436. doi:10.1112/plms/s2-23.1.428.
[40] S. C. Miller, R. H. Good, A wkb-type approximation to the schrödinger equation, Phys. Rev. 91 (1953) 174–179. doi:10.1103/PhysRev.91.174.
[41] N. Balazs, One dimensional band theory in the wkb approximation, Annals of Physics 53 (3) (1969) 421 – 438. doi:10.1016/0003-4916(69)90033-5.
[42] A. D. Pierce, Physical interpretation of the wkb or eikonal approximation for waves and vibrations in inhomogeneous beams and plates, The Journal of the Acoustical Society of America 48 (1B) (1970) 275–284. doi:10.1121/1.1912125.
[43] A. T. Fabro, N. S. Ferguson, T. Jain, R. Halkyard, B. R. Mace, Wave propagation in one-dimensional waveguides with slowly varying random spatially correlated variability, Journal of Sound and Vibration 343 (Supplement C) (2015) 20 – 48. doi:10.1016/j.jsv.2015.01.013.
[44] A. Caldeira, A. Leggett, Quantum tunnelling in a dissipative system, Annals of Physics 149 (2) (1983) 374 – 456. doi:10.1016/0003-4916(83)90202-6.
[45] R. B. Nielsen, N. Peake, Tunnelling effects for acoustic waves in slowly varying axisymmetric flow ducts, Journal of Sound and Vibration 380 (2016) 180–191. doi:10.1016/j.jsv.2016.06.003.
[46] S. Iyer, C. M. Will, Black-hole normal modes: A wkb approach. i. foundations and application of a higher-order wkb analysis of potential-barrier scattering, Phys. Rev. D 35 (1987) 3621–3631. doi:10.1103/PhysRevD.35.3621.
[47] R. Nielsen, S. Sorokin, The WKB approximation for analysis of wave propagation in curved rods of slowly varying diameter, Proc. R. Soc. A 470 (2167) (2014) 20130718. doi:10.1098/rspa.2013.0718.
URL http://rspa.royalsocietypublishing.org/content/470/2167/20130718
[48] J. O. Morsbøl, S. V. Sorokin, N. Peake, A WKB approximation of elastic waves travelling on a shell of revolution, Journal of Sound and Vibration 375 (Supplement C) (2016) 162–186. doi:10.1016/j.jsv.2016.04.001.
[49] A. T. Fabro, N. S. Ferguson, B. R. Mace, Flexural Wave Propagation in Slowly Varying Random Waveguides Using a Finite Element Approach, Journal of Physics: Conference Series 744 (1) (2016) 012198. doi:10.1088/1742-6596/744/1/012198.

[50] A. T. Fabro, D. Beli, J. R. F. Arruda, N. S. Ferguson, B. Mace, Uncertainty analysis of band gaps for beams with periodically distributed resonators produced by additive manufacturing, in: ISMA 2016 Conference on Noise and Vibration Engineering, Leuve, Belgium, 2016, p. 12.
[51] A. T. Fabro, N. S. Ferguson, B. R. Mace, Wave propagation in slowly varying waveguides using a finite element approach, Journal of Sound and Vibration 442 (2019) 308–329. doi:10.1016/j.jsv.2018.11.004.
[52] R. Ghanem, P. D. Spanos, Stochastic Finite Elements: A Spectral Approach, revised edition Edition, Dover Publications, Minneola, N.Y., 2012.
[53] P. W. Anderson, Absence of Diffusion in Certain Random Lattices, Physical Review 109 (5) (1958) 1492–1505. doi:10.1103/PhysRev.109.1492.
[54] Y. K. Lin, G. Q. Cai, Probabilistic structural dynamics: Advanced theory and applications, McGraw-Hill, New York, 1995.
[55] D. Beli, J. R. de França Arruda, Influence of additive manufacturing variability in elastic band gaps of beams with periodically distributed resonators, in: Proceedings of the $3^{r}d$ Symposium on Uncertainty Quantification and Stochastic Modeling, ABCM, 2016, p. 10. doi:10.20906/CPS/USM-2016-0019.
[56] M. Ruzzene, A. Baz, Attenuation and localization of wave propagation in periodic rods using shape memory inserts, Smart Materials and Structures 9 (6) (2000) 805. doi:10.1088/0964-1726/9/6/310.
[57] J. F. M. Scott, The statistics of waves propagating in a one-dimensional random medium, Proceedings of the Royal Society of London. Series A, Mathematical and Physical Sciences 398 (1985) 341–363, 1815.
[58] A. Luongo, On the amplitude modulation and localization phenomena in interactive buckling problems, International Journal of Solids and Structures 27 (15) (1991) 1943–1954. doi:10.1016/0020-7683(91)90187-K.
[59] A. Luongo, Mode localization by structural imperfections in one-dimensional continuous systems, Journal of Sound and Vibration 155 (2) (1992) 249–271. doi:10.1016/0022-460X(92)90510-5.
[60] D. Mogilevtsev, F. A. Pinheiro, R. R. dos Santos, S. B. Cavalcanti, L. E. Oliveira, Suppression of Anderson localization of light and Brewster anomalies in disordered superlattices containing a dispersive metamaterial, Physical Review B 82 (8) (2010) 081105. doi:10.1103/PhysRevB.82.081105.
[61] D. Mogilevtsev, F. A. Pinheiro, R. R. dos Santos, S. B. Cavalcanti, L. E. Oliveira, Light propagation and Anderson localization in disordered superlattices containing dispersive metamaterials: Effects of correlated disorder, Physical Review B 84 (9) (2011) 094204. doi:10.1103/PhysRevB.84.094204.
[62] J. Zhu, Y. Chen, X. Zhu, F. J. Garcia-Vidal, X. Yin, W. Zhang, X. Zhang, Acoustic rainbow trapping, Scientific Reports 3 (2013) 1728. doi:10.1038/srep01728.
[63] Y. Y. Chen, R. Zhu, M. V. Barnhart, G. L. Huang, Enhanced flexural wave sensing by adaptive gradient-index metamaterials, Scientific Reports 6 (2016) 35048. doi:10.1038/srep35048.
[64] H. Meng, D. Chronopoulos, A. T. Fabro, Optimal design of a rainbow metamaterial, in: Proceedings of the 26th International Congress on Sound and Vibration - ICSV26, Montreal, Canada, 2019.
[65] D. Yu, Y. Liu, G. Wang, H. Zhao, J. Qiu, Flexural vibration band gaps in timoshenko beams with locally resonant structures, Journal of Applied Physics 100 (12) (2006) 124901. doi:10.1063/1.2400803.
[66] A. Qureshi, B. Li, K. T. Tan, Numerical investigation of band gaps in 3d printed cantilever-in-mass metamaterials, Scientific Reports 6 (2016) 28314. doi:10.1038/srep28314.
[67] G. Trainiti, J. Rimoli, M. Ruzzene, Wave propagation in periodically undulated beams and plates, International Journal of Solids and Structures 75–76 (2015) 260 – 276. doi:10.1016/j.ijsolstr.2015.08.019.
[68] J. O. Morsbøl, S. V. Sorokin, N. Peake, A WKB approximation of elastic waves travelling on a shell of revolution, Journal of Sound and Vibration 375 (Supplement C) (2016) 162–186. doi:10.1016/j.jsv.2016.04.001.
URL http://www.sciencedirect.com/science/article/pii/S0022460X16300189
[69] S.-K. Lee, B. Mace, M. Brennan, Wave propagation, reflection and transmission in non-uniform one-dimensional waveguides, Journal of Sound and Vibration 304 (1) (2007) 31 – 49. doi:10.1016/j.jsv.2007.01.039.
[70] M. Petyt, Introduction to Finite Element Vibration Analysis, 2nd Edition, Cambridge University Press, Cambridge, 2010.
[71] D. Duhamel, B. Mace, M. Brennan, Finite element analysis of the vibrations of waveguides and periodic structures, Journal of Sound and Vibration 294 (1) (2006) 205 – 220. doi:10.1016/j.jsv.2005.11.014.
[72] J. M. Mencik, M. N. Ichchou, A substructuring technique for finite element wave propagation in multi-layered systems, Computer Methods in Applied Mechanics and Engineering 197 (6) (2008) 505–523. doi:10.1016/j.cma.2007.08.002.
[73] Y. Waki, B. Mace, M. Brennan, Numerical issues concerning the wave and finite element method for free and forced vibrations of waveguides, Journal of Sound and Vibration 327 (1) (2009) 92 – 108. doi:https://doi.org/10.1016/j.jsv.2009.06.005.
[74] J.-M. Mencik, On the low- and mid-frequency forced response of elastic structures using wave finite elements with one-dimensional propagation, Computers & Structures 88 (11) (2010) 674 – 689. doi:https://doi.org/10.1016/j.compstruc.2010.02.006.
[75] Y. Waki, On the application of finite element analysis to wave motion in one-dimensional waveguides, phd, University of Southampton (Dec. 2007).
URL https://eprints.soton.ac.uk/52061/
[76] B. R. Mace, E. Manconi, Wave motion and dispersion phenomena: Veering, locking and strong coupling effects, The Journal of the Acoustical Society of America 131 (2) (2012) 1015–1028. doi:10.1121/1.3672647.
URL https://asa.scitation.org/doi/10.1121/1.3672647
[77] A. T. Fabro, N. S. Ferguson, T. Jain, R. Halkyard, B. R. Mace, Wave propagation in one-dimensional waveguides with slowly varying random spatially correlated variability, Journal of Sound and Vibration 343 (2015) 20–48. doi:10.1016/j.jsv.2015.01.013.
[78] S. P. Huang, S. T. Quek, K. K. Phoon, Convergence study of the truncated Karhunen–Loeve expansion for simulation of stochastic processes, International Journal for Numerical Methods in Engineering 52 (2001) 1029–1043. doi:10.1002/nme.255.
[79] A. T. Fabro, N. S. Ferguson, B. R. Mace, Structural vibration analysis with random fields using the hierarchical finite element method, Journal of the Brazilian Society of Mechanical Sciences and Engineering 41 (2) (2019) 80. doi:10.1007/s40430-019-1579-0.

[80] Y. Waki, B. R. Mace, M. J. Brennan, Free and forced vibrations of a tyre using a wave/finite element approach, Journal of Sound and Vibration 323 (3–5) (2009) 737–756. doi:10.1016/j.jsv.2009.01.006.
[81] C. Sugino, S. Leadenham, M. Ruzzene, A. Erturk, On the mechanism of bandgap formation in locally resonant finite elastic metamaterials, Journal of Applied Physics 120 (13) (2016) 134501. doi:10.1063/1.4963648.
[82] Y. Xiao, J. Wen, D. Yu, X. Wen, Flexural wave propagation in beams with periodically attached vibration absorbers: Band-gap behavior and band formation mechanisms, Journal of Sound and Vibration 332 (4) (2013) 867–893. doi:10.1016/j.jsv.2012.09.035.
[83] P. F. Pai, Metamaterial-based Broadband Elastic Wave Absorber, Journal of Intelligent Material Systems and Structures 21 (5) (2010) 517–528. doi:10.1177/1045389X09359436.
[84] M. I. Hussein, M. J. Leamy, M. Ruzzene, Dynamics of Phononic Materials and Structures: Historical Origins, Recent Progress, and Future Outlook, Applied Mechanics Reviews 66 (4) (2014) 040802–040802. doi:10.1115/1.4026911.
[85] B. R. Mace, Discussion of "Dynamics of Phononic Materials and Structures: Historical Origins, Recent Progress and Future Outlook" (Hussein, M. I., Leamy, M. J., and Ruzzene, M., 2014, ASME Appl. Mech. Rev., 66(4), p. 040802), Applied Mechanics Reviews 66 (4) (2014) 045502–045502. doi:10.1115/1.4027723.
[86] M. I. Hussein, M. J. Leamy, M. Ruzzene, Closure to "Discussion of 'Dynamics of Phononic Materials and Structures: Historical Origins, Recent Progress, and Future Outlook'" (Hussein, M. I., Leamy, M. J., and Ruzzene, M., 2014, ASME Appl. Mech. Rev., 66(4), p. 040802), Applied Mechanics Reviews 66 (4) (2014) 046002–046002–1. doi:10.1115/1.4027795.
[87] H. Meng, D. Chronopoulos, A. T. Fabro, W. Elmadih, I. Maskery, Rainbow metamaterials for broadband multi-frequency vibration attenuation: Numerical analysis and experimental validation, Journal of Sound and Vibration 465 (2020) 115005. doi:10.1016/j.jsv.2019.115005.
[88] J. Heading, An Introduction to Phase-Integral Methods, reprinted Edition, Dover Publications, New York, USA, 2013.
[89] R. S. Langley, N. S. Bardell, P. M. Loasby, The optimal design of near-periodic structures to minimize vibration transmission and stress levels, Journal of Sound and Vibration 207 (5) (1997) 627–646. doi:10.1006/jsvi.1997.1116.
[90] H. Meng, D. Chronopoulos, A. T. Fabro, I. Maskery, Y. Chen, Optimal design of rainbow elastic metamaterials, International Journal of Mechanical Sciences (2019) 105185doi:10.1016/j.ijmecsci.2019.105185.
URL http://www.sciencedirect.com/science/article/pii/S0020740319322568
[91] D. Cardella, P. Celli, S. Gonella, Manipulating waves by distilling frequencies: a tunable shunt-enabled rainbow trap, Smart Materials and Structures 25 (8) (2016) 85017. doi:10.1088/0964-1726/25/8/085017.
URL https://doi.org/10.1088%2F0964-1726%2F25%2F8%2F085017
[92] T. J. Sullivan, Introduction to Uncertainty Quantification, 1st Edition, Vol. 63 of Texts in Applied Mathematics, Springer, Switzerland, 2015.
[93] G. I. Schuëller, H. J. Pradlwarter, Uncertain linear systems in dynamics: Retrospective and recent developments by stochastic approaches, Engineering Structures 31 (11) (2009) 2507–2517. doi:10.1016/j.engstruct.2009.07.005.
[94] M. M. Kaminski, Computational Mechanics of Composite Materials: Sensitivity, Randomness and Multiscale Behaviour, Springer, London, 2005.
[95] Z. Hu, S. Mahadevan, Uncertainty quantification and management in additive manufacturing: current status, needs, and opportunities, The International Journal of Advanced Manufacturing Technology 93 (5-8) (2017) 2855–2874. doi:10.1007/s00170-017-0703-5.
[96] M. R. Machado, S. Adhikari, J. M. C. Dos Santos, J. R. F. Arruda, Estimation of beam material random field properties via sensitivity-based model updating using experimental frequency response functions, Mechanical Systems and Signal Processing 102 (Supplement C) (2018) 180–197. doi:10.1016/j.ymssp.2017.08.039.
[97] Y. Li, Y. Xu, Research on the effects of geometrical and material uncertainties on the band gap of the undulated beam, AIP Advances 7 (9) (2017) 095315. doi:10.1063/1.5000979.
[98] G. Stefanou, The stochastic finite element method: Past, present and future, Computer Methods in Applied Mechanics and Engineering 198 (2009) 1031–1051, 9–12. doi:10.1016/j.cma.2008.11.007.
[99] K. K. Phoon, S. P. Huang, S. T. Quek, Simulation of second-order processes using Karhunen–Loeve expansion, Computers & Structures 80 (12) (2002) 1049–1060. doi:10.1016/S0045-7949(02)00064-0.
[100] K. K. Phoon, H. W. Huang, S. T. Quek, Simulation of strongly non-Gaussian processes using Karhunen–Loeve expansion, Probabilistic Engineering Mechanics 20 (2) (2005) 188–198. doi:10.1016/j.probengmech.2005.05.007.
[101] W. Betz, I. Papaioannou, D. Straub, Numerical methods for the discretization of random fields by means of the Karhunen–Loève expansion, Computer Methods in Applied Mechanics and Engineering 271 (2014) 109–129. doi:10.1016/j.cma.2013.12.010.
[102] C. Li, A. Der Kiureghian, Optimal discretization of random fields, Journal of Engineering Mechanics 119 (6) (1993) 1136–1154. doi:10.1061/(ASCE)0733-9399(1993)119:6(1136).
[103] R. Rubinstein, D. Kroese, Simulation and the Monte Carlo method, second edition Edition, Wiley Series in Probability and Statistics, John Wiley & Sons, Inc., Hoboken, NJ, USA, 2007.
[104] A. M. J. Olsson, G. E. Sandberg, Latin Hypercube Sampling for Stochastic Finite Element Analysis, Journal of Engineering Mechanics 128 (1) (2002). doi:10.1061/(ASCE)0733-9399(2002)128:1(121).